Acta Biomaterialia xxx (2018) xxx–xxx

Contents lists available at ScienceDirect

Acta Biomaterialia

journal homepage: www.elsevier.com/locate/actabiomat

Full length article

Biodegradation of ECM hydrogel promotes endogenous brain tissue restoration in a rat model of stroke

Harmanvir Ghuman [a,b], Carrinton Mauney [c], Julia Donnelly [d], Andre R. Massensini [a,g], Stephen F. Badylak [a,b,e], Michel Modo [a,b,f,*]

[a] University of Pittsburgh, McGowan Institute for Regenerative Medicine, Pittsburgh, PA, USA
[b] Department of Bioengineering, Pittsburgh, PA, USA
[c] Department of Neuroscience, Pittsburgh, PA, USA
[d] Department of Biological Sciences, Pittsburgh, PA, USA
[e] Department of Surgery, Pittsburgh, PA, USA
[f] Department of Radiology, Pittsburgh, PA, USA
[g] Universidade Federal de Minas Gerais, Department of Physiology and Biophysics, Belo Horizonte, Brazil

ARTICLE INFO

Article history:
Received 9 July 2018
Received in revised form 12 September 2018
Accepted 14 September 2018
Available online xxxx

Keywords:
Extracellular matrix
Hydrogel
Magnetic resonance imaging
Stroke
Regeneration
Tissue repair
Biodegradation
Biomaterial
Scaffold
Cell invasion

ABSTRACT

The brain is considered to have a limited capacity to repair damaged tissue and no regenerative capacity following injury. Tissue lost after a stroke is therefore not spontaneously replaced. Extracellular matrix (ECM)-based hydrogels implanted into the stroke cavity can attract endogenous cells. These hydrogels can be formulated at different protein concentrations that govern their rheological and inductive properties. We evaluated histologically 0, 3, 4 and 8 mg/mL of porcine-derived urinary bladder matrix (UBM)-ECM hydrogel concentrations implanted in a 14-day old stroke cavity. Less concentrated hydrogels (3 and 4 mg/mL) were efficiently degraded with a 95% decrease in volume by 90 days, whereas only 32% of the more concentrated and stiffer hydrogel (8 mg/mL) was resorbed. Macrophage infiltration and density within the bioscaffold progressively increased in the less concentrated hydrogels and decreased in the 8 mg/mL hydrogels. The less concentrated hydrogels showed a robust invasion of endothelial cells with neovascularization. No neovascularization occurred with the stiffer hydrogel. Invasion of neural cells increased with time in all hydrogel concentrations. Differentiation of neural progenitors into mature neurons with axonal projections was evident, as well as a robust invasion of oligodendrocytes. However, relatively few astrocytes were present in the ECM hydrogel, although some were present in the newly forming tissue between degrading scaffold patches. Implantation of an ECM hydrogel partially induced neural tissue restoration, but a more complete understanding is required to evaluate its potential therapeutic application.

Statement of Significance

Extracellular matrix hydrogel promotes tissue regeneration in many peripheral soft tissues. However, the brain has generally been considered to lack the potential for tissue regeneration. We here demonstrate that tissue regeneration in the brain can be achieved using implantation of ECM hydrogel into a tissue cavity. A structure-function relationship is key to promote tissue regeneration in the brain. Specifically, weaker hydrogels that were retained in the cavity underwent an efficient biodegradation within 14 days post-implantation to promote a tissue restoration within the lesion cavity. In contrast, stiffer ECM hydrogel only underwent minor biodegradation and did not lead to a tissue restoration. Inductive hydrogels weaker than brain tissue provide the appropriate condition to promote an endogenous regenerative response that restores tissue in a cavity. This approach offers new avenues for the future treatment of chronic tissue damage caused by stroke and other acute brain injuries.

* Corresponding author at: University of Pittsburgh, McGowan Institute for Regenerative Medicine, 3025 East Carson St, Pittsburgh, PA 15203, USA.
E-mail address: mmm154@pitt.edu (M. Modo).

https://doi.org/10.1016/j.actbio.2018.09.020
1742-7061/

1. Introduction

Tissues and organs have a varied intrinsic ability to repair and regenerate [1]. Although the liver can efficiently regenerate tissue from only 25% of its volume [2], the brain is generally considered to have a limited capacity to repair damaged tissue [3] and is believed to have no potential to regenerate lost tissue [4–6]. Following injuries, such as stroke or traumatic brain injury, cells and extracellular matrix (ECM) are phagocytosed and removed from the lesion core to produce a cavity filled with extracellular fluid (ECF) [7]. Typically, this stroke cavity is fully formed by 2 weeks post-injury and is surrounded by glial scarring that delineates this lesion core from the peri-infarct tissue [8]. Following stroke, most neurons are lost in the peri-infarct area, but cytoarchitectural changes are also observed, such as astrocytosis [9]. A long-lasting repair response occurs with peri-infarct angiogenesis and neural stem cell (NSC) migration along blood vessels from the sub-ependymal zone into damaged tissues [10]. However, neither this endogenous reparative response [10], nor transplantation of NSCs [11], restore functional brain tissue within the cavity.

Preclinical rodent studies using fetal tissue implanted into the stroke cavity showed the formation of new tissue [12,13], including efferent and afferent axonal projections [14–16], and evidence of improvement of behavioral deficits [17], with a 2–3 week post-lesion implantation time point favoring survival and integration of cells [12]. Fetal tissue contains neural progenitors and stem cells, as well as blood vessels, embedded within donor ECM. In contrast to implantation of NSCs in suspension [11], NSCs within an ECM hydrogel were retained within the stroke cavity [18], highlighting the structural importance of ECM. In the areas of ECM hydrogel that did not contain the implanted NSCs, host cells infiltrated the hydrogel, consistent with the known inductive properties of the biomaterial [18]. In contrast to synthetic hydrogels, ECM bioscaffolds have been shown to produce an inductive remodeling response to promote functional tissue restoration [19,20].

ECM bioscaffolds can be sourced from different organs, such as the urinary bladder matrix (UBM) [21–25], umbilical cord [26], peripheral nervous system [27], spinal cord [28], as well as the brain [21,24,29]. Pre-gel ECM preparations are cytocompatible, while enhancing proliferation and migration of neural progenitors [21,22]. Typically, ECM bioscaffolds induce a shift in macrophage phenotypes leading to a pro-repair response [23,30] that affects tissue-specific cells, such as neurons [24]. A comparison of different ECM sources revealed the largest increase in differentiation and neurite outgrowth of neural progenitors with UBM-ECM rather than central nervous system (CNS)-derived ECM [21,24]. These in vitro results suggest that heterologous organ sources potentially exert a greater pro-repair effect than CNS-derived ECM. In the spinal cord, UBM-ECM performed as well as spinal cord-derived ECM, but provided favorable degradation kinetics [28]. Non-gelling UBM- and brain-ECM injections after traumatic brain injury revealed improvements in behavioral deficits, further highlighting their potential for therapeutic CNS applications [31,32]. Sourcing of homologous CNS tissues is however challenging, considering the low yield of ECM compared to other tissue, such as UBM [24]. In humans only post-mortem CNS material would be available to decellularize and formulate as hydrogel. Use of xenogenic tissue sources, such as pigs, provides an economical and logistically advantageous approach compared to human material [24]. In the present study, we therefore explored if porcine-derived UBM-ECM hydrogel implantation in the injured rat brain could induce a prolonged endogenous tissue restoration response.

Magnetic resonance imaging (MRI) was used to determine the volume and specific central nervous system (CNS) location for injection of the soluble precursor form (i.e. pre-gel) of an ECM hydrogel using an injection-drainage approach [33]. Concentrations >3 mg/mL ECM will gel *in situ* and provide a substrate for endogenous cell invasion. A marked macrophage infiltration occurs within 24 h with >300,000 cells inside the 8 mg/mL ECM hydrogel. Most macrophages activate toward an M2-like, or regulatory and anti-inflammatory phenotype [34]. This 8 mg/mL preparation also attracted more neural progenitors, oligodendrocytes and endothelial cells than lower concentrations. The 8 mg/mL hydrogel reduced lesion volume by 11% over 90 days, but did not impact behavioral deficits [35]. Unlike ECM in peripheral organs, where the bioscaffold is typically completely replaced between 75 and 90 days [36–40], there was a slow degradation of the ECM hydrogel in the brain with only a 32% reduction in volume by 90 days [35]. Only a sparse population of cells, including macrophages, remained within the bioscaffold. Bioscaffold stiffness and an insufficient sustained host tissue response could limit biodegradation and prevent tissue restoration [41,42].

Although a higher concentration 8 mg/mL ECM induces greater cell infiltration acutely due to its higher inductive content, we hypothesized that weaker hydrogels long-term would afford a greater cell density in the bioscaffold and improve biodegradation. We further surmised that an efficient biodegradation was required to promote tissue restoration. The objective of the present study was to determine the time course (1, 14, 90 days) of cell invasion and biodegradation of different concentrations (3, 4, 8 mg/mL) of ECM hydrogel in a stroke cavity. Restoration of site-appropriate, functional tissue within the stroke cavity would indicate that the brain has the capacity to self-repair and create *de novo* tissue, but that appropriate conditions need to be engineered to facilitate this process.

2. Methods

2.1. Extracellular matrix (ECM) hydrogel

ECM hydrogel was produced by isolating the basement membrane and tunica propria of porcine urinary bladder (Tissue Source, Inc., Lafayette, IN) by mechanical delamination [25]. Decellularization was performed by immersing the isolated layers of the bladder in 0.1% peracetic acid in ethanol with agitation (4% v/v; 120 min; 300 rpm). A series of PBS and deionized water rinses removed cellular debris [25]. Decellularization was confirmed using Hematoxylin & Eosin, 4′,6-diamidino-2-phenylindole (DAPI) staining, agarose gel electrophoresis, and quantification of remnant DNA [43]. ECM was then lyophilized, comminuted, and solubilized with pepsin (1 mg/mL) in 0.01 N HCl. pH neutralization was achieved by adding 0.1 N NaOH. Approximately 70% of the urinary bladder matrix (UBM) is collagen [29], but other prominent ECM proteins, such as fibronectin, decorin, laminin subunit γ1 are also present [44]. A variety of growth factors are also retained within the UBM-ECM preparation, including transforming growth factor-β, vascular endothelial growth factor-A, basic fibroblast growth factor, and nerve growth factor [21], all of which are known to influence neuronal and endothelial cells. In addition, matrix-bound nanovesicles (MBV) enriched in miRNA and other signaling molecules are present within the ECM preparation [45].

Dilution to a desired concentration (3, 4 and 8 mg/mL) was attained by mixture of lyophilized ECM pepsin digest stock (10 mg/mL) with the appropriate volume of PBS [25]. Gelation of this preparation is concentration, pH and temperature-dependent. Concentrations <3 mg/mL do not readily form a hydrogel on the bench [33]. Four and 8 mg/mL preparations have a viscosity of 0.084 and 0.443 Pa s and reach 50% gelation in 3.2 and 3 min, respectively [33]. Storage modulus (G′) for both 4 mg/mL (76.6 Pa) and 8 mg/mL (460.4 Pa) exceeded their loss modulus

Please cite this article in press as: H. Ghuman et al., Biodegradation of ECM hydrogel promotes endogenous brain tissue restoration in a rat model of stroke, Acta Biomater. (2018), https://doi.org/10.1016/j.actbio.2018.09.020

(G″, 11.0 Pa and 66.4 Pa, respectively). The 8 mg/mL preparation approximates the reported 500–1000 Pa elastic modulus of healthy brain tissue [46–48].

2.2. Middle cerebral artery occlusion (MCAo)

All animal procedures complied with the US Animals Welfare Act (2010) and were approved by the University of Pittsburgh Institutional Animal Care and Use Committee (IACUC). Sprague-Dawley rats (male, 260 ± 15 g, Taconic Labs, USA) were maintained on a 12-hour light/dark schedule, with food and water available *ad libitum*. For transient intraluminal right middle cerebral artery (MCA) occlusion, a rat model of stroke, a 5-0 silicone rubber-coated monofilament (diameter 0.12 mm, length 30 mm, tip coating at 0.35 mm for 5–6 mm, Doccol, USA) was advanced to the ostium of the MCA in the circle of Willis, while the animal was under isoflurane anesthesia (4% induction, 1% maintenance in 30% O_2). The MCA was occluded for 70 min prior to reperfusion by retracting the filament to the common carotid bifurcation, producing an occlusion similar to the scenario in 2/3 of all cases of human ischemic stroke. After recovery from anesthesia, animals were assessed for forelimb flexion and contralateral circling. Buprenorphine (0.05 mg/kg) was administered to the animals twice daily for 3 days. Daily post-operative care and neurological assessment were performed until they recovered pre-operative weight [49,50]. Animals not exhibiting signs of MCA damage (i.e. unilateral forelimb flexion) or who failed to recover weight were excluded from the study.

2.3. Magnetic resonance imaging (MRI)

Acquisition: To assess the presence, location and volume of tissue loss, MCAo rats were anesthetized with isoflurane (4% induction, 1% maintenance in 30% O_2) and scanned using a T_2-weighted spin-echo MRI sequence (TR = 6000 ms, TE = 8 ms, 8 Averages, FOV 30 × 30 mm, 128 × 128 matrix, 42 slices at 0.5 mm thickness) on a horizontal bore 9.4 T Varian scanner 10 days post-infarction [33,51].

Lesion volume and intensity measurements: Stroke damage was defined as tissue with a hyperintense signal on T_2-weighted images that were thresholded at 1 standard deviation above the mean of a rectangular region of interest (ROI) in the contralateral hemisphere, encompassing striatum, corpus callosum and neocortex [52,53]. As detailed in Ghuman et al. [35], rats (n = 56) with lesion volume >40 mm^3 (i.e. 40 μL) were randomly assigned to either the untreated or the ECM treated groups, resulting in an equivalent distribution of lesion volumes (range: 41–236 μL) across all groups. Rats with signs of hemorrhage were excluded.

Table 1
Animals per experimental condition.

Conditions	Day 1	Day 14	Day 90
0 mg/mL	3	5	5
3 mg/mL	5	5	4
4 mg/mL	5	5	5
8 mg/mL	5	5	5

2.4. Implantation procedure

Fourteen days post-stroke, rats underwent ECM implantation by placement into a stereotactic frame (Kopf, USA) under isoflurane anesthesia (4% induction, 1% maintenance in 30% O_2). A vertical skin incision exposed Bregma on the skull and provided guidance for the location of two Burr holes for 1) the placement of a 250 μL Hamilton syringe with a 24 G beveled tip metal needle (Hamilton) filled with solubilized ECM in PBS, as well as 2) a hole for a drainage cannula (24 G) [33]. MR images of lesion location and volumes were used to define stereotactic coordinates for needle/cannula placements. Needles/cannula were advanced into the stroke lesion cavity. Lesion-equivalent volumes of solubilized ECM (41–236 μL) were slowly injected into the ventral posterior region of the cavity to displace and drain the less dense necrotic debris from the stroke cavity, as previously described [33]. Injection of solubilized ECM (0, 3, 4, 8 mg/mL concentrations, Table 1) was controlled using a frame mounted injection pump (World Precision Instruments, USA) at a constant speed of 10 μL/min until the total volume was delivered (4–24 min). The solubilized ECM formed a hydrogel *in situ* at 37 °C body temperature. Needle and cannula were left in place for 5 min to allow material to dissipate and form a gel before the needles were slowly withdrawn from the brain. Burr holes were filled with bone wax (Fisher) prior to suturing. LX4 (Ferndale, containing 4% Lidocaine) was topically applied as an analgesic, and buprenorphine (0.05 mg/kg) was administered via intraperitoneal injection to provide sustained pain relief.

2.5. Histologic analyses

Perfusion-fixation of tissue: To determine the in-situ distribution of the ECM hydrogel and cell infiltration within the hydrogel, rats were transcardially perfused at 1, 14 or 90 days post-implantation with 0.9% saline followed by 4% paraformaldehyde (in 0.2 M PBS) to fix brain tissue prior to its removal from the skull. Brains were post-fixed in 4% paraformaldehyde for 24 h prior to being cryopreserved in 30% sucrose with sodium azide (Sigma) at 4 °C. Histologic sections (50 μm thickness) were prepared on a cryostat (Leica) and placed directly onto microscopic slides to preserve tissue morphology.

Immunohistochemistry: Brain sections were washed 3 × 5 min with 0.01 M PBS, followed by 1 hr permeabilization in PBS + 0.1% Triton X-100 (Sigma) at room temperature (21 °C). Primary antibodies (Table 2) were applied, diluted in PBS + 0.05% Triton X-100, and incubated at 4 °C overnight. After rinsing off the primary antibodies (3 × 5 min PBS), appropriate secondary AlexaFluor 488, 555, or 660 antibodies (1:500; Life Technologies) were applied for

Table 2
List of antibodies used for immunohistochemistry.

Antibody	Concentration	Company	Cat. Ref.	Clone
Collagen-I	1:250	Abcam	Ab34710	Collagen I aa 1–1464
Iba-1	1:300	Abcam	Ab5076	Iba1 aa 135–147
GFAP	1:3000	Sigma	G3893	G-A-5
DCX	1:150	Abcam	Ab153668	CAA0661'7.1 and AAT58219.1
CNPase	1:200	Abcam	Ab6319	11-5B
Fox3	1:500	Abcam	Ab104224	1B7
RECA-1	1:100	Abcam	Ab9774	RECA-1
CD86	1:200	Abcam	Ab53004	EP1159Y
CD206	1:200	Santa Cruz	sc-34577	C-20

Please cite this article in press as: H. Ghuman et al., Biodegradation of ECM hydrogel promotes endogenous brain tissue restoration in a rat model of stroke, Acta Biomater. (2018), https://doi.org/10.1016/j.actbio.2018.09.020

1 h at room temperature followed by 3 × 5 min washes with PBS. Finally, sections were coverslipped with Vectashield for fluorescence containing Hoechst 33342 (1 μg/mL, Sigma) and stored at 4 °C prior to imaging. Visualization of antibodies was performed with a fluorescence microscope (Axioimager M2, Zeiss) interfaced with a monochrome camera driven by Stereo Investigator image capture software (MBF Bioscience) using a motorized stage [33].

ECM hydrogel volume: The virtual tissue module (MBF Bioscience) tiled individual 20× magnification images to create a composite whole brain slice. Anterior-posterior whole biomaterial images (500 μm apart) were acquired to measure the area occupied by ECM (i.e. collagen I staining), and then multiplied by the distance between images to approximate total volume [35]. The rate of biodegradation was calculated by obtaining the average ECM hydrogel volume at a reference time point (1 or 14 days) and dividing it with the volume at the target time point (14 or 92 days). Degradation rate was defined as μL/day.

Lesion and parenchyma volume: Regions of Interest (ROIs) were drawn on 8-bit whole brain histology images of DAPI in Fiji version 1.49 (https://fiji.sc) around the tissue for each hemisphere, including the ventricles. Based on the pixel intensity in the contralateral hemisphere, a threshold was applied to define parenchyma and create a binary map [35]. For each histological slice, contralateral parenchyma was defined by subtracting the lateral ventricle. Ipsilateral parenchyma volume was defined by subtracting lateral ventricle and lesion volume. Total volumes were calculated by multiplying area measurements by the distance to the next slice (500 μm). A ratio between ipsi- and contralateral parenchymal and ventricular volumes was calculated.

Tissue deformation: ROIs were defined based on anatomical definitions to segment host tissue and determine if ECM implantation affected the deformation of the brain due to stroke damage [35]. A midline shift is commonly observed due to the host tissue expanding due to the lack of sufficient structural support, resulting from the void of the lesion cavity [54,55]. Midline shift was determined by placing a vertical line from the longitudinal fissure to the median eminence at Bregma +0.7, which commonly is the central slice of MCAo damage [35]. In the middle of the vertical line, perpendicular lines are drawn to measure the distance to the edge of each hemisphere. A ratio is taken of these two measurements to define the relative midline shift. Ventricular enlargement is also often seen as a consequence of tissue deformations. Volume changes of tissue parenchyma were also calculated to determine if stroke and ECM implantation affected structural changes in these regions.

Glial scarring: Brain tissue sections were immunolabeled for glial fibrillary acid protein (GFAP) before acquiring whole brain images at 10× magnification, as previously described [35]. Images were acquired with 100 ms exposure time for all animals to provide consistent signal intensity across all sections. The images were then processed through Fiji to define straight lines as ROIs starting from the lesion boundary and drawing away from the cavity. A plot of intensity versus distance determined thickness of the glial scar in both cortex and striatum. The average intensity of the GFAP signal was then averaged and binned for every 200 μm, starting from the lesion boundary. ROIs were drawn in all anterior-posterior brain sections containing the glial scar.

Peri-infarct astrocytosis: Whole brain GFAP stained images were first converted to 8-bit images before applying a threshold to mask GFAP+ cells and create a binary map to determine the area covered by astrocytes in both ipsilateral (i.e. right) stroke-affected and contralateral (i.e. left) unaffected hemispheres [35]. The same threshold value was used for all brain sections to maintain consistency. ROIs were then drawn around the parenchyma of the ipsilateral hemisphere to determine the area fraction (%) represented by astrocytes.

Cell invasion: Collagen I was used to delineate the border between host and biomaterial [33–35,56] to determine the number and phenotype of cells invading the injected ECM. Whole graft images were acquired at 20× magnification with brain sections stained for Hoechst (to identify cell nuclei) and Collagen I (to mask and delineate the host-ECM boundary to quantify cell invasion. Images were processed through Fiji to define grayscale images of the invading cells. Composite images of the biomaterial were untiled before quantifying the number of invading cells in Cell Profiler version 2.1.1 (http://cellprofiler.org).

Cell phenotypes: Images were acquired at 20× magnification to determine the total number of cells (i.e. Hoechst+) within the ECM material and to determine the phenotype of cells [34,35]. Five to eight images were acquired at equally-spaced distances throughout the material within a section and counted across all anterior-posterior slices containing ECM hydrogel. Phenotypic markers for neural progenitor cells (doublecortin, DCX), neurons (Fox3), astrocytes (glial fibrillary acid protein, GFAP), oligodendrocytes (2′,3′-cyclic-nucleotide 3′-phospodiesterase, CNPase), endothelial cells (rat endothelial cell antigen 1, RECA-1), microglia (ionized calcium-binding adapter molecule 1, Iba-1), as well as macrophage activation (CD206 for the M2 phenotype, CD86 for M1 phenotype) were used for analysis (Table 2). Although many mononuclear macrophages share histologic markers, Iba-1 is a commonly used marker for brain microglia [57]. Phenotypes were expressed as % of total cells present to account for differences in the number of invading cells.

2.6. Statistical analyses

Statistical analyses were performed in SPSS 17 for Mac (IBM) with significance set at $p < 0.05$. Specifically, two-way ANOVAs were used to compare group and time effects as independent variables, with tissue volumes, cell invasion and phenotypes as dependent variables. Bonferroni post-hoc tests validated overall significant comparisons. A LOWESS spline curve fitting was performed on the ECM volume data to represent the expected time line of biodegradation. Pearson correlations were calculated to determine associations between two dependent variables. To establish how concentration affects the relationship between these variables, data from 3, 4 and 8 mg/mL ECM concentrations were pooled for each time point. Graphs were drawn in Prism 7 (GraphPad) with data points representing the mean and bars reflecting the standard deviation.

3. Results

3.1. Weaker ECM hydrogels undergo efficient biodegradation and reduce tissue cavitation

ECM hydrogel stiffness is dependent on protein concentration [33]. The 8 mg/mL ECM preparation resulted in a stiffer bioscaffold that was consistently still present by 90 days post-implantation while filling the entire lesion cavity (Fig. 1A). However, less concentrated gels (3 and 4 mg/mL) revealed extensive degradation by 14 days and an almost complete resorption of implanted material by 90 days. A key difference between 3 and 4 mg/mL gels compared to the stiffer 8 mg/mL gels was that the less concentrated ECM hydrogels displaced smaller amounts of damaged tissue. In cases of non-communicating tissue voids, the 3 mg/mL hydrogels did not fully cover areas of cavitation. An anterior-posterior view of the lesion cavity pre-implantation showed a distinct delineation of the newly formed tissue inside the original lesion void at 90 days (Fig. 1B). ECM hydrogel within the tissue void provides a scaffold that bridges the space between host tissue. The bioscaffold contains cells that invaded the substrate to re-colonize the cavity (Fig. 1C). Lateral ventricles were enlarged in all animals, indicating

Please cite this article in press as: H. Ghuman et al., Biodegradation of ECM hydrogel promotes endogenous brain tissue restoration in a rat model of stroke, Acta Biomater. (2018), https://doi.org/10.1016/j.actbio.2018.09.020

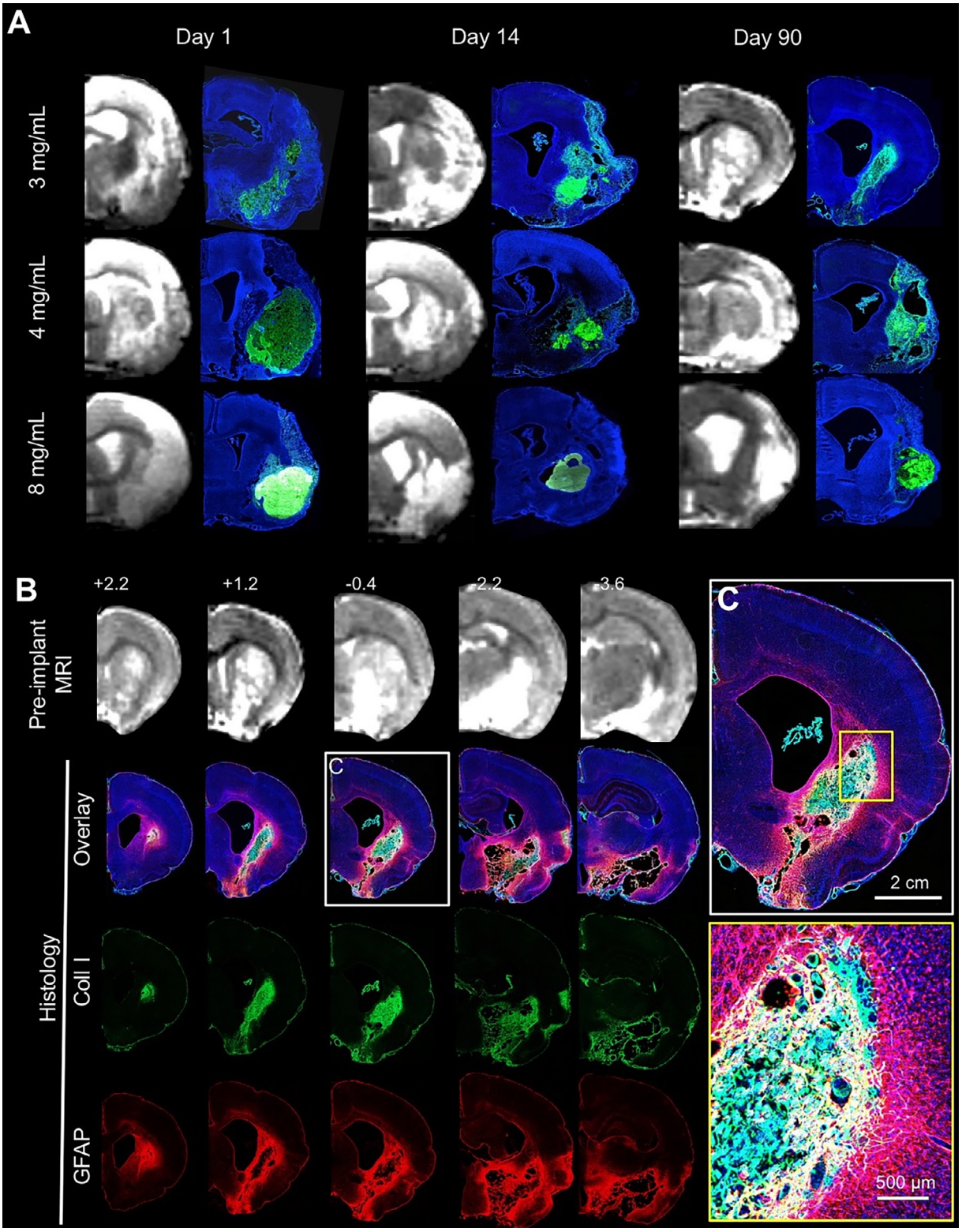

Fig. 1. Macroscopic distribution of ECM hydrogel in the stroke cavity. A. Pre-implantation T_2-weighted magnetic resonance images (MRI) were used to define stereotactic coordinates and calculate volumes of ECM hydrogel precursor for injection. A complete coverage of the lesion cavity with an ECM bioscaffold (Collagen I in green, DAPI in Blue) was achieved with this approach. A concentration of 8 mg/mL ECM shows limited degradation over 90 days, whereas 3 and 4 mg/mL show a very efficient structural remodeling, with only a small amount of hydrogel being present at the final time point. B. Anterior-Posterior pre-implantation MRI scans revealed the location and volume of the lesion cavity for comparison with 4 mg/mL ECM hydrogel at 90 days post-implantation. Active tissue remodeling inside the ECM bioscaffold and around the lesion cavity is evident (DAPI in Blue, Collagen I in green, GFAP in red). C. At the lesion-tissue boundary, astrocytes (GFAP+ cells) cross the glial scar and invade the bioscaffold that is replacing the stroke cavity. Capillary-like structures were also apparent in ECM remodeling regions. (For interpretation of the references to colour in this figure legend, the reader is referred to the web version of this article.)

Please cite this article in press as: H. Ghuman et al., Biodegradation of ECM hydrogel promotes endogenous brain tissue restoration in a rat model of stroke, Acta Biomater. (2018), https://doi.org/10.1016/j.actbio.2018.09.020

some degree of hydrocephalus *ex vacuo*, which is known to occur after volumetric tissue loss. In animals with sub-cortical lesions, ECM hydrogel appeared to be pulling tissue together, whereas in large lesions that included cortical regions such contractions of tissue did not occur.

A volumetric MRI comparison of lesion volume prior to implantation of hydrogel showed no significant differences between ECM concentrations ($F = 0.23$, n.s.) at different time points ($F = 1.032$, n.s.; Fig. 2A). Animals within each group therefore suffered a similar severity of stroke, with lesion volume pre-implantation ranging between 41 and 236 μL. The histologic evaluation of hydrogel volume at different time points showed an overall group effect ($F = 27.0$, $p < 0.001$), with 0 mg/mL (PBS) being significantly different from all other groups (Fig. 2B). ECM volumes at 1 day post-implantation were not significantly different from each other, but 3 and 4 mg/mL volumes were lower compared to 8 mg/mL, further confirming qualitative observations that stiffer gels achieved a greater displacement of damaged tissues within the cavity in addition to filling the tissue voids. A significant interaction ($F = 3.085$, $p < 0.05$) between ECM concentrations and time was also evident. The 8 mg/mL concentration was significantly ($p < 0.01$) different from 3 and 4 mg/mL on day 14 and 90. The 3 and 4 mg/mL groups showed no statistically significant difference in their biodegradation dynamics. The 4 mg/mL hydrogel underwent the fastest degradation in the first two weeks at a rate of 6.11 μL/day (Table 3). In contrast, the 8 mg/mL preparation only saw a biodegradation

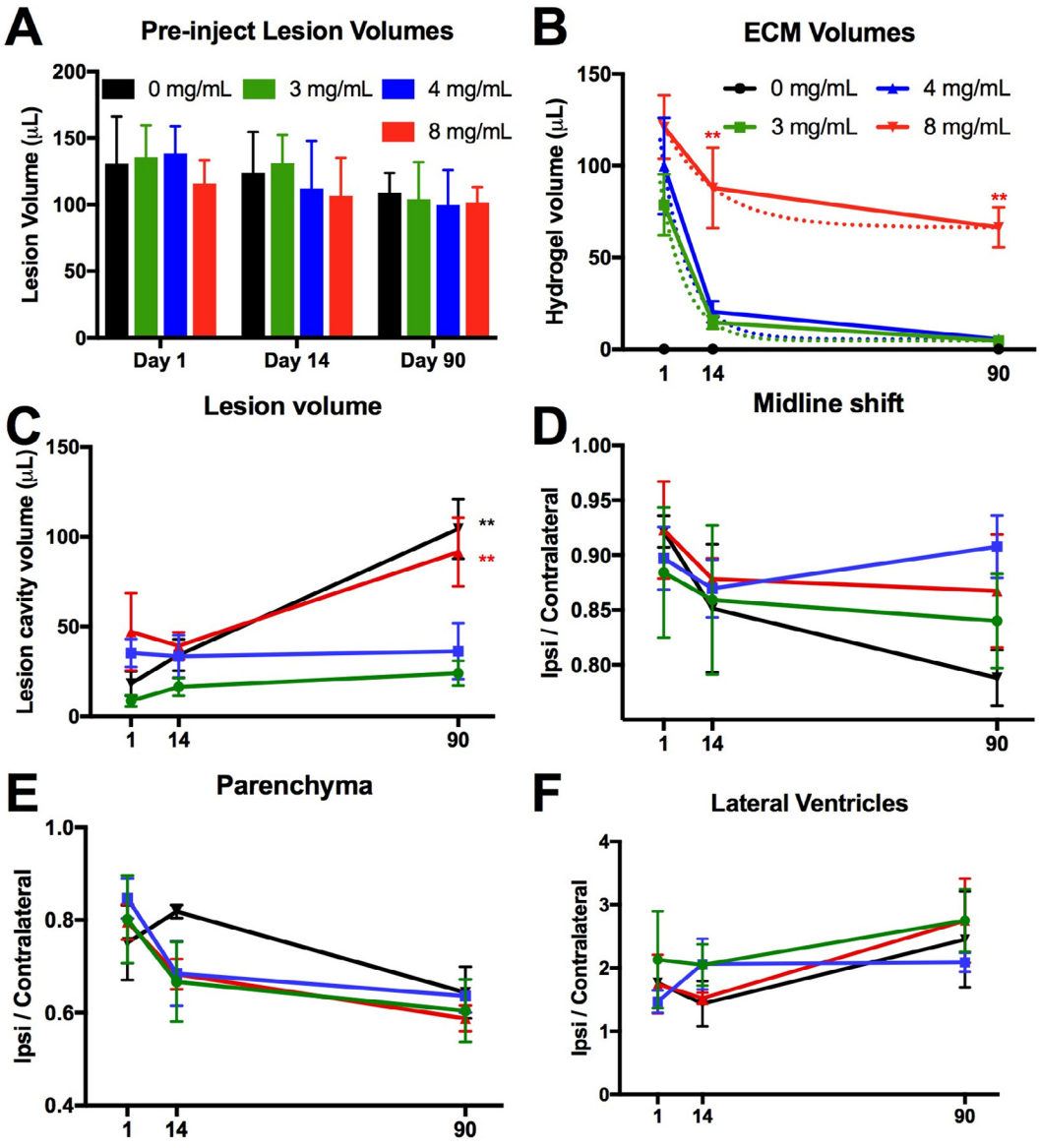

Fig. 2. ECM biodegradation and tissue deformation. A. Lesion volumes calculated from T_2-weighted MR images acquired 4 days before ECM injection (10 days post-stroke) were used to assign rats to groups with equivalent lesion volumes. B. Remaining volume of ECM hydrogel was quantified to determine biodegradation at 1, 14 and 90 days post-implantation. At 90 days post-implantation a decrease in ECM volume of 94.1%, 95%, and 32% was recorded in the 3, 4, and 8 mg/mL. A locally weighted scatter plot smoother (LOWESS) fitted curve visualize the anticipated degradation pattern with a 3 mg/mL concentration providing a half-life of 4.5 days, the 4 mg/mL 4.9 days and 8 mg/mL >90 days. A biodegradation plateau is reached for the 3 and 4 mg/mL concentration around 28 days, whereas the 8 mg/mL concentration plateaued at 66 days. C. Less concentrated 3 and 4 mg/mL ECM concentrations halted lesion progression, whereas the 8 mg/mL had a more limited impact on the evolution of the cavity compared to no treatment (0 mg/mL). D. Midline shift was calculated by a ratio between distance of the ipsi- and contralateral hemisphere midpoints. A gradual shift of the midline was evident in all groups. The 4 mg/mL condition exhibited the most promise to reduce tissue deformation. E. Hydrogel implantation did not affect the imbalance in ipsi- and contralateral parenchymal volumes that follows a stroke. F. There was also no effect on the hydrocephalus ex vacuo that ensues as a result of stroke damage, as evidence by the ratio of the ipsi- and contralateral lateral ventricles. ($^{**}p < 0.01$).

Please cite this article in press as: H. Ghuman et al., Biodegradation of ECM hydrogel promotes endogenous brain tissue restoration in a rat model of stroke, Acta Biomater. (2018), https://doi.org/10.1016/j.actbio.2018.09.020

Table 3
Biodegradation rate of different ECM concentrations.

Concentration	3 mg/mL	4 mg/mL	8 mg/mL
1–14 days	4.92 μL/day	6.11 μL/day	2.54 μL/day
14–90 days	0.13 μL/day	0.19 μL/day	0.28 μL/day
1–90 days	0.83 μL/day	1.06 μL/day	0.61 μL/day

rate of 2.54 μL/day, i.e. approximately half the rate of the 3 and 4 mg/mL hydrogels.

A difference between the 8 mg/mL concentration hydrogel and the less concentrated formulations was also evident for its potential to reduce lesion volume (Fig. 2C). The 3 and 4 mg/mL hydrogel concentrations very effectively reduced lesion progression ($F = 9.171$, $p < 0.001$). Lesion progression without treatment (0 mg/mL) showed an increase in lesion volume over 90 days. However, an 8 mg/mL concentration reduced this progression. No significant difference between groups was evident at 1 and 14 days post-implantation, but 3 and 4 mg/mL significantly reduced lesion volume at 90 days ($F = 5.414$, $p < 0.01$). ECM hydrogel-treated animals exhibited no significant overall reduction in midline shift compared to untreated (0 mg/mL) animals (Fig. 2D). Furthermore, ECM hydrogel treatment did not have a significant effect on parenchymal volume (Fig. 2E) or lateral ventricle volumes (Fig. 2F).

3.2. Glia scarring and astrocytosis are unaffected by ECM hydrogel implantation

To evaluate the host tissue glial response to ECM hydrogel implantation, glial scarring was measured in the striatum and cortex (Fig. 3A). It was noted qualitatively that only minor scarring was evident 1 day post-implantation and that a defined astrocytic barrier was more evident at 14 days (Fig. 3B). By 90 days in the 3 and 4 mg/mL, no defined line of an astrocytic scar was evident, but this area transformed into a wider area of reactive astrocytes. Quantification of scarring within the striatum showed no significant difference between groups ($F = 2.42$, n.s.) or distance ($F = 4.53$, n.s.) at day 1 post-implantation (Fig. 3C). At 14 days, scarring was more pronounced compared to day 1 for all groups at the cavity border ($F = 90.13$, $p < 0.001$), but it was equivalent for all groups ($F = 0.09$, n.s.). At 90 days, a wider area of reactive astrocytes defined the cavity border, significantly decreasing in density as a function of distance from the stroke cavity ($F = 14.44$, $p < 0.001$) in all groups ($F = 1.54$, n.s.). A similar pattern of results was also evident in the cortex with a scarring distance effect at 14 ($F = 62.05$, $p < 0.001$) and 90 days ($F = 31.31$, $p < 0.001$), but no group differences at any time point. In addition to glial scarring, reactive astrocytes were found in the peri-infarct area (Fig. 3D). A quantification of these revealed a significant increase between day 1 and 14 for all groups ($F = 25.23$, $p < 0.001$, Fig. 3E). As ECM concentration was not related to the increase in number of reactive astrocytes ($F = 0.6015$, n.s.), changes in astrocytosis are likely related to the stroke pathology, rather than implantation of ECM hydrogel.

3.3. ECM hydrogel efficiently promotes endogenous cell invasion with an increased cell density in less concentrated scaffolds

Although the glial scar is often seen as an obstacle to regeneration, there was a substantial cell invasion into ECM hydrogel for all concentrations (Fig. 4). A quantification of cells within the bioscaffold was achieved by defining the ECM hydrogel using collagen I staining, which is significantly higher in the implanted biomaterial compared to the host brain (Fig. 5A). Individual cell nuclei were counted across all sections containing ECM hydrogel. In absolute numbers, the 8 mg/mL ECM hydrogel contained the most cells at day 1 (average 366278), whereas the 3 mg/mL preparation attracted 4× fewer cells (average 96267, $F = 3.522$, $p < 0.05$, Fig. 5B). This pattern was consistent for all time points ($F = 6.748$, $p < 0.01$) with the 4 mg/mL condition initially attracting more cells and then rapidly decreasing to the level of the 3 mg/mL ECM hydrogels. However, the total number of invading cells is also affected by ECM hydrogel volume. As ECM hydrogel is rapidly degraded in the 3 and 4 mg/mL condition, but not in the 8 mg/mL condition, total cell invasion does not reflect the qualitative impression of cell content within the bioscaffold. Cell density within the ECM reflects this consideration and indicates that for the 8 mg/mL ECM hydrogel, cell density decreases with time, reflecting the slower biodegradation observed by 90 days (Fig. 5C). In contrast, the 4 mg/mL condition provides a consistent cell density indicating the mode of action for the more rapid biodegradation and tissue replacement ($F = 4.065$, $p < 0.05$). In the 3 mg/mL condition, cell density increased over time to reach the level of the 4 mg/mL hydrogel, potentially reflecting the lower inductive potential of this concentration and weaker support for cell migration. An efficient cell invasion was typically accompanied by blood vessels in degrading ECM hydrogel (Fig. 5D), as well as by a large number of astrocytes and macrophages occupying this intermittent space (Fig. 5E).

3.4. Macrophage density affects biodegradation

The invasion of host cells into ECM hydrogel is dominated by macrophages. Invasion of these phagocytic cells occurs through the peri-infarct tissue across the glial scarring (Fig. 6A). Iba-1 cells are present with distinct morphological characteristics, such as a rounded or amoeboid shape, but also filopodia shapes with processes protruding into their surroundings (Fig. 6B). M1- (CD86+) and M2-like (CD206+) activation markers further distinguish macrophage phenotypic activity within the bioscaffold (Fig. 6C). A quantification of the proportion of macrophages within the ECM hydrogel showed that the 8 mg/mL concentration consistently contained a higher percentage of Iba-1 + macrophages compared to the other concentrations, increasing to approximately 50% over time ($F = 13.37$, $p < 0.001$, Fig. 6D). The 3 and 4 mg/mL concentrations only contained about 30% macrophages at any time point and showed faster biodegradation than the 8 mg/mL concentration. Total macrophage invasion mirrored the total cell invasion, with 8 mg/mL containing a significantly greater quantity of cells compared to day 1 at all time points ($F = 9.577$, $p < 0.001$). Macrophage density within the ECM hydrogel showed a gradual decrease in the 8 mg/mL condition, while the 4 mg/mL concentration showed a consistent density of 700–800 cells/μL ($F = 3.297$, $p < 0.05$). This quantification of cells was also reached and maintained by the 3 mg/mL preparation at 14 days post-implantation. A phenotypic shift in macrophages was evident with a large proportion (35–48%) showing M1-like characteristics at day 1, especially in the lower ECM concentrations ($F = 23.21$, $p < 0.001$, Fig. 6E). The 8 mg/mL hydrogel had significantly fewer M1-like proinflammatory macrophages at day 1 (~20% of all invading cells) with only a minimal decrease over time to reach the same level (~10%) as the 3 and 4 mg/mL bioscaffolds. A shift in phenotypic activation from M1-like macrophages at day 1 to M2-like at day 14 was evident with over 20% of cells showing M2-like characteristics for the 3 and 8 mg/mL group and 11.6% for the 4 mg/mL preparation ($F = 10.25$, $p < 0.001$) compared to <4% of cells having only a M2-like marker expression at day 1 and 90 ($F = 128.8$, $p < 0.001$). With time ($F = 15.77$, $p < 0.001$), co-expression of M1- and M2-like cell markers increased consistently for all groups, with 27–33% of cells co-expressing both markers ($F = 2.06$, n.s.).

Please cite this article in press as: H. Ghuman et al., Biodegradation of ECM hydrogel promotes endogenous brain tissue restoration in a rat model of stroke, Acta Biomater. (2018), https://doi.org/10.1016/j.actbio.2018.09.020

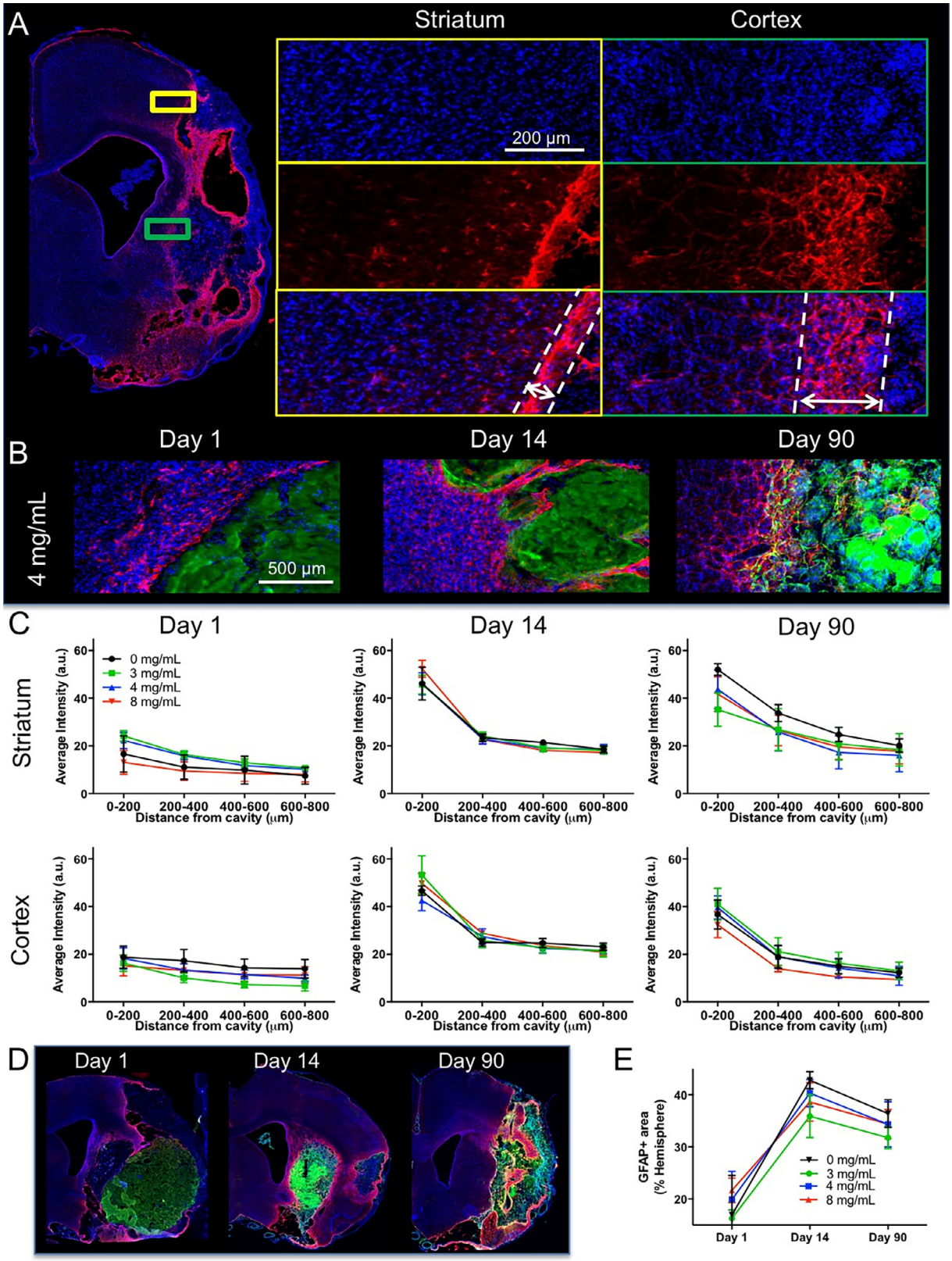

Fig. 3. Glial scarring and tissue astrocytosis. A. To evaluate the impact of ECM hydrogel on glial scarring at the tissue interface, whole brain slices covering the lesion cavity were acquired to measure the level of astrocytic (GFAP) reactivity in the striatal and cortical tissues. A 4 mg/mL concentration condition is shown here. B. However, it is important to note a clear morphological difference in astrocytic activity at the different time points, with the 14 day time point showing the sharpest interface border, whereas by 90 days post-implantation a complex mesh of astrocytic processes blurring the line between established and regenerating tissue. C. A quantitative comparison indicated a marked increase in GFAP intensity at the border of the cavity 1 day post-implantation that was equivalent for all groups. A gradual decrease of reactivity away from the cavity border was evident. The highest increase in astrocyte reactivity was observed at 14 days post-implantation with a surge in intensity reaching further into both striatum and cortex. By 90 days, the extent and intensity of glial reactivity was reducing, but not back to the level present on day 1. D. peri-infarct astrocytosis was extensive in areas surrounding the ECM hydrogel implantation at all time points. E. A quantitative comparison mirrored the results of glial scarring, where an increase occurred in the 14 days post-implantation. This was nevertheless equivalent between all groups, including the 0 mg/mL condition indicating that this astrocytosis is not related to the ECM hydrogel, but either due to lesion progression or the implantation procedure. The 3 mg/mL condition exhibited the lowest level of astrocytosis, potentially revealing a minor effect of ECM permeating into peri-infarct tissue.

Please cite this article in press as: H. Ghuman et al., Biodegradation of ECM hydrogel promotes endogenous brain tissue restoration in a rat model of stroke, Acta Biomater. (2018), https://doi.org/10.1016/j.actbio.2018.09.020

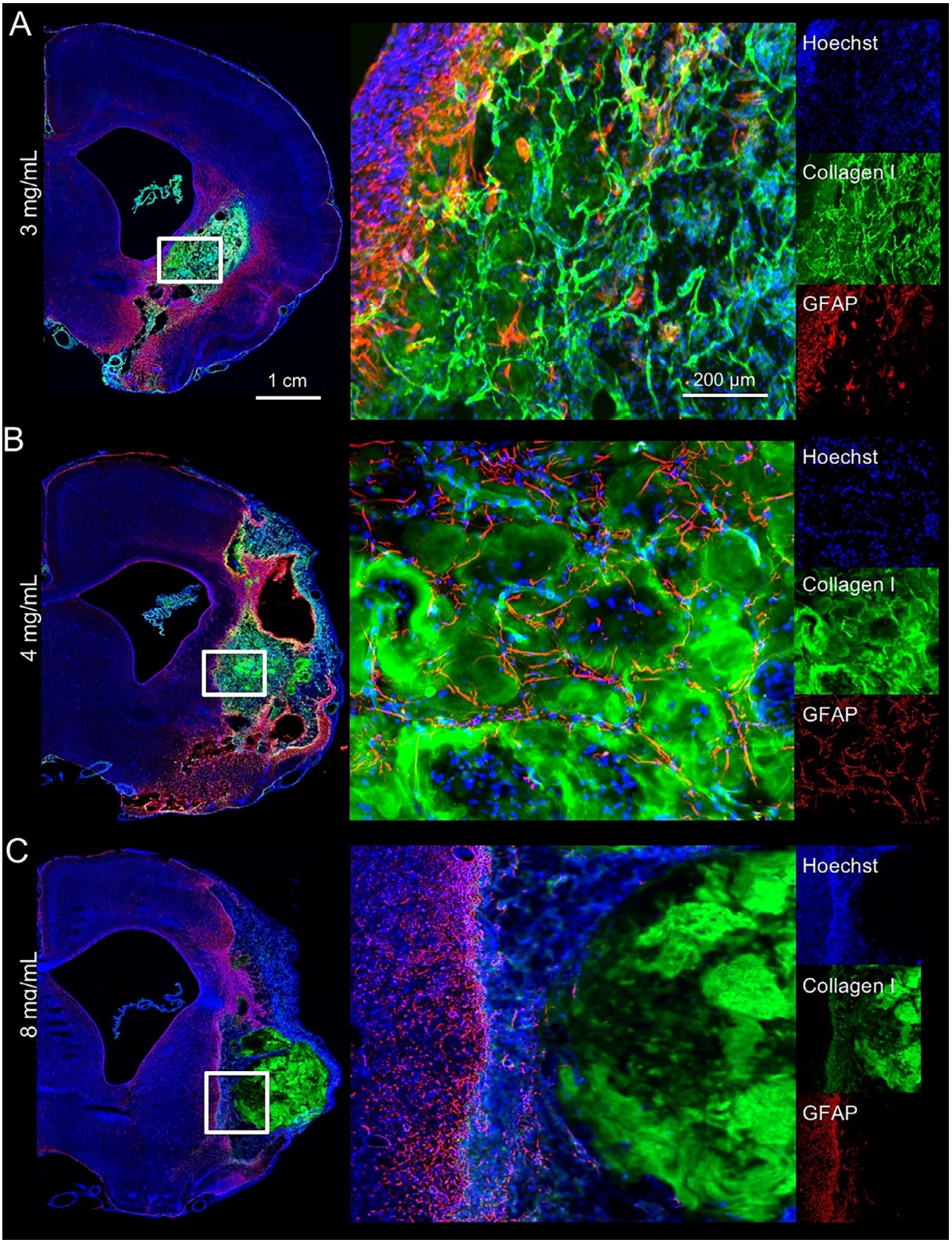

Fig. 4. Biodegradation of the material is crucial for supporting cell infiltration and tissue remodeling. Biodegradation of ECM hydrogel is concentration dependent with less concentrated 3 and 4 mg/mL bioscaffolds getting efficiently degraded, whereas the 8 mg/mL persists longer. A. At Day 90, a very small amount (5.9%) of the 3 mg/mL ECM was present with host cells showing an excellent invasion and structural remodeling. An even distribution of the invading GFAP+ cells is seen throughout the remaining hydrogel. B. With 4 mg/mL, chain cell invasion can be seen with GFAP+ cells filling the space in between patches of ECM hydrogel, as identified by collagen I staining. C. In contrast with these less concentrated hydrogels, a sharp boundary between the biomaterial and host was evident in animals injected with 8 mg/mL. Density of cells in the hydrogel at 90 days was much lower compared to the less concentrated gels. These observations highlight key differences in biodegradation and cell infiltration between different concentrations of ECM hydrogel.

Please cite this article in press as: H. Ghuman et al., Biodegradation of ECM hydrogel promotes endogenous brain tissue restoration in a rat model of stroke, Acta Biomater. (2018), https://doi.org/10.1016/j.actbio.2018.09.020

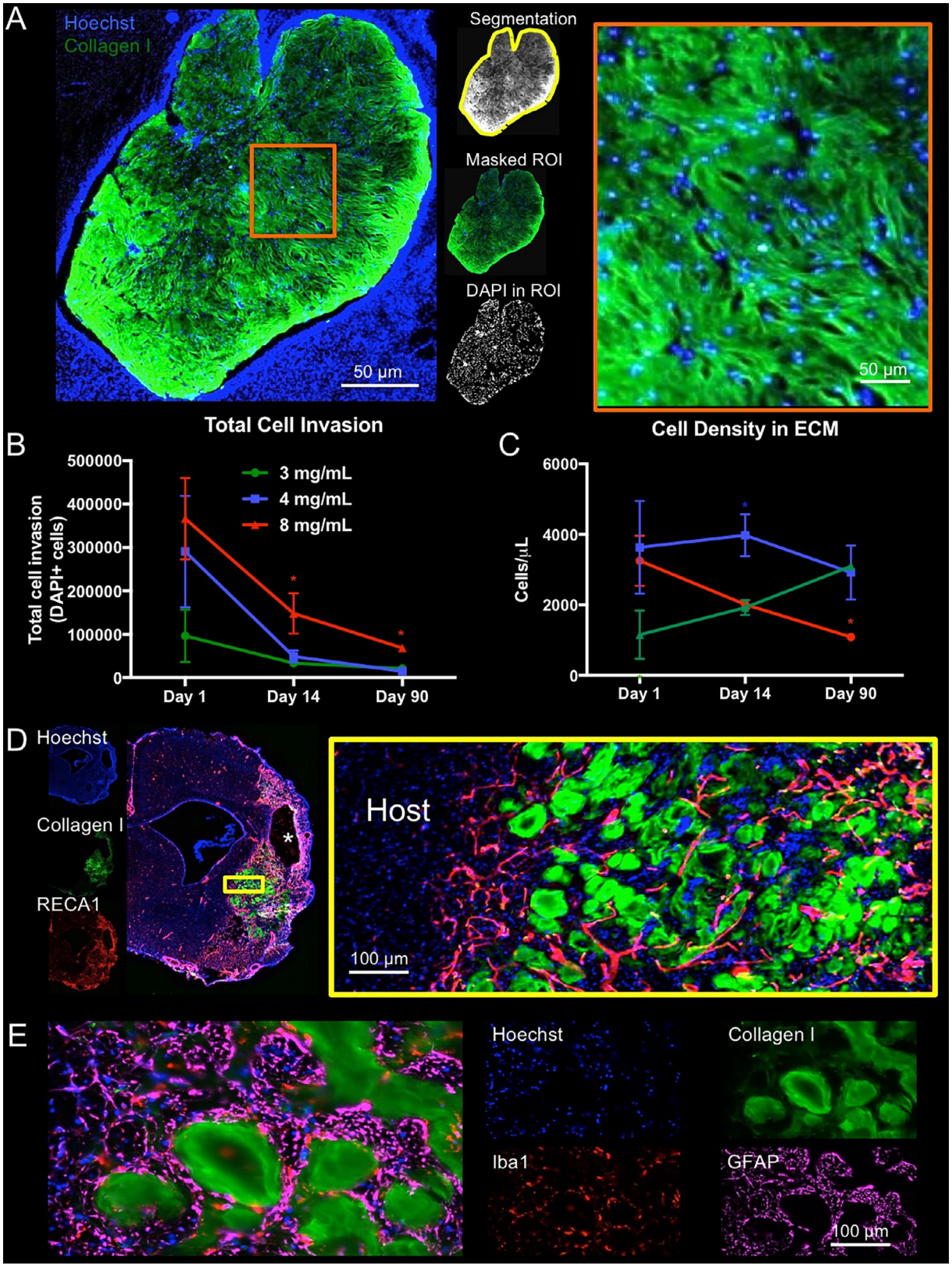

Fig. 5. Presence of host cells in ECM hydrogel. A. Using collagen I staining, a region of interest (ROI) was defined around the edges of the biomaterial (8 mg/mL shown) and applied to the DAPI image to provide a quantification of the number of cells present within the hydrogel. B. Total cell infiltration indicated that the 8 mg/mL hydrogel consistently contained the highest number of cells. In all conditions, a gradual decrease in total number of cells is seen that is related to the biodegradation of the scaffold. C. To account for ECM hydrogel volume changes due to biodegradation, cell density was calculated. The 4 mg/mL hydrogel concentration provided a very consistent density of approximately 4000 cells/μL. Cell density for the 8 mg/mL decreased from a 4 mg/mL comparable level, whereas 3 mg/mL increased to a comparable level at 90 days. These cell density dynamics reveal key differences in the inductive potential of ECM hydrogel concentrations. D. Cell infiltration and density here focus on the bioscaffold content (4 mg/mL shown). However, a significant number of cells are evident within the previous cavity in between patches of ECM hydrogel. E. Iba-1+ macrophages and GFAP+ astrocytes are common phenotypes, but no scar or foreign body response was evident. ($^{*}p < 0.05$).

Please cite this article in press as: H. Ghuman et al., Biodegradation of ECM hydrogel promotes endogenous brain tissue restoration in a rat model of stroke, Acta Biomater. (2018), https://doi.org/10.1016/j.actbio.2018.09.020

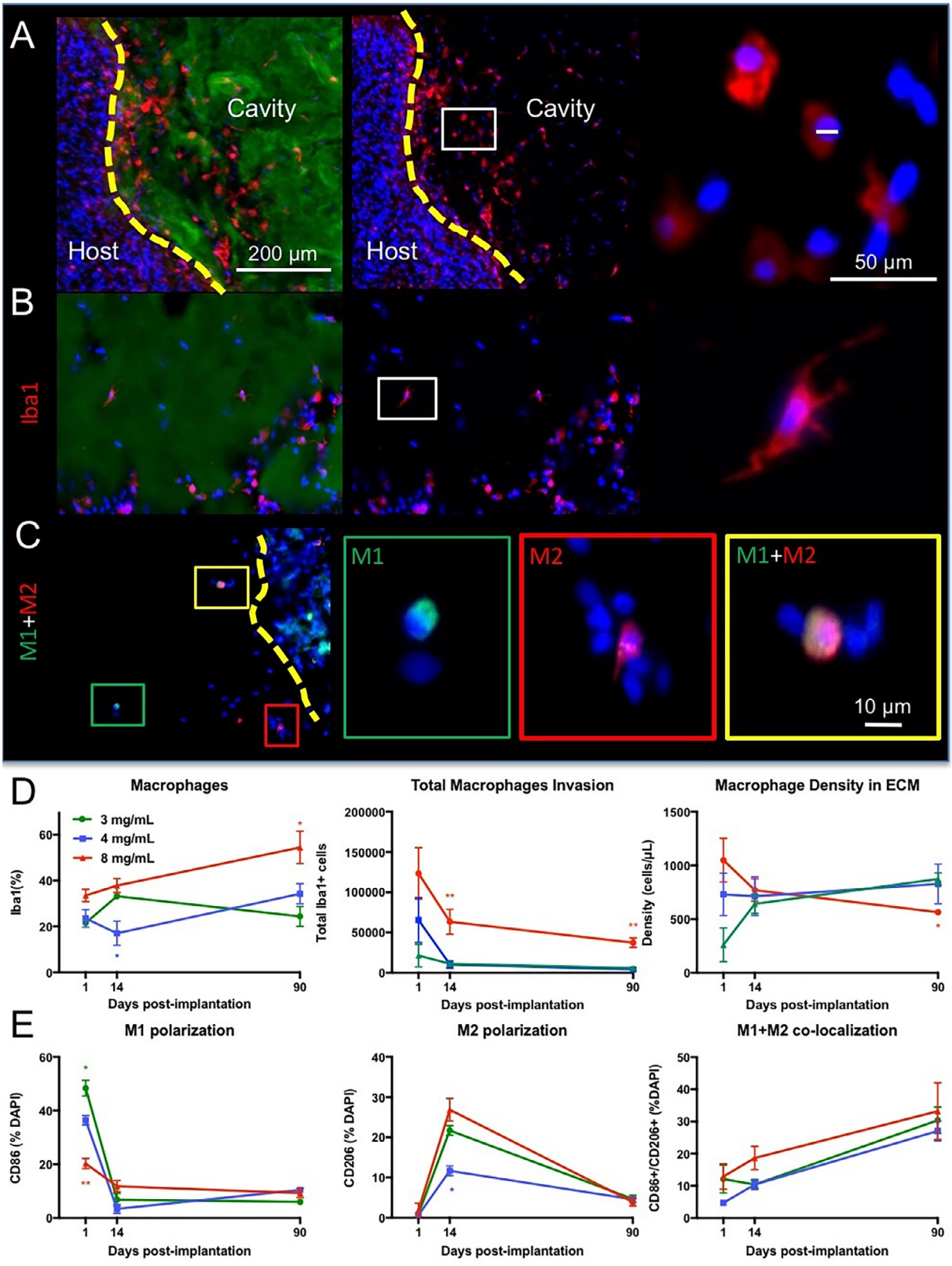

Fig. 6. Phenotypic characterization of invading immune cells in ECM hydrogel. A. Invasion of Iba-1+ macrophage is evident at the tissue/hydrogel interface (4 mg/mL). Collagen I staining of the ECM hydrogel defined the region of analysis of macrophage invasion. Individual leader cells spread through the material, typically with an amoeboid shape, 1 day post-implantation. B. At 14 days post-implantation, clusters of Iba-1 positive cells were increasingly common, with some macrophages exhibiting an activated and ramified morphology. C. M1-like (CD86) and M2-like (CD206) polarization of macrophages was also evident with some cells expressing both markers, especially at 90 days. D. The 8 mg/mL ECM concentration invoked the highest proportion of macrophage and this increased with time. However, the total number of macrophage gradually decreased in all conditions. Density of macrophages within efficiently degrading hydrogel was high and persisted at approximately 700–800 cells/μL. Only in the 8 mg/mL ECM hydrogel was there a decrease in macrophage density. E. Analysis of polarization of macrophages indicated that M1-like phenotypes were predominant 1 day post-implantation, but that M2-like cells were common 14 days post-implantation. By 90 days, both M1 and M2 were commonly found in the same macrophage cell. ($^{*}p < 0.05$; $^{**}p < 0.01$).

Please cite this article in press as: H. Ghuman et al., Biodegradation of ECM hydrogel promotes endogenous brain tissue restoration in a rat model of stroke, Acta Biomater. (2018), https://doi.org/10.1016/j.actbio.2018.09.020

3.5. An efficient neovascularization occurs in less concentrated ECM hydrogels

Neovascularization is necessary to ensure the long-term survival of invading cells. In the 8 mg/mL ECM hydrogel, very few blood vessels were evident. In contrast, neovascularization was evident in the 3 and 4 mg/mL bioscaffold by 90 days, including branching of different vessels inside and in between the ECM hydrogel (Fig. 7A). In some cases, very tortuous structures were present (Fig. 7B), similar to angiogenesis in some peri-infarct areas post-stroke. The number of endothelial (i.e. RECA1+) cells invading the ECM hydrogel (Fig. 7C) was quantified to determine the cellular basis for neovascularization. The small percentage of endothelial cells that invaded the hydrogel 1 day post-implantation appeared to follow specific trails inside the ECM. No significant difference between ECM concentrations was evident at 1 day post-implantation (Fig. 7D). An inflection point occurred at 14 days, with infiltration peaking for the 8 mg/mL ($F = 8.794$, $p < 0.001$). An increase to 30% of all cells being endothelial cells occurred in the 3 mg/mL concentration. In contrast, only 4.8% of cells within the 8 mg/mL hydrogel were of an endothelial phenotype by 90 days post-implantation. The lack of endothelial cell invasion beyond 14 days in the 8 mg/mL hydrogel indicates a key shift in the cellular response of cells at this time point. Neovascularization in the 3 and 4 mg/mL concentrations at 90 days contrasts starkly with the lack of new blood vessels in the 8 mg/mL ECM preparation.

3.6. Neural cells infiltrate the ECM hydrogel

Although macrophages and endothelial cell invasion are associated with biodegradation and vascularization of the ECM hydrogel, neural cells are required to produce *de novo* brain tissue. The infiltration of neural progenitor (DCX+) cells is evident in the peri-infarct area, as well as within the degrading ECM hydrogel (Fig. 8A). Neural progenitors were present in the ECM hydrogel as early as 1 day post-implantation. The neural progenitor cells mature into neurons (b-III-tubulin+ and/or NeuN+) and astrocytes (GFAP+) in the degrading bioscaffold (Fig. 8B and C). Small pockets of tissue developed within the degrading bioscaffold and presented conditions that allowed for maturation of brain cells (Fig. 8D), including the formation of axonal projections as determined by neurofilament staining (Fig. 8E). Neuronal cells were typically accompanied by astrocytes and oligodendrocytes (Fig. 8F), even when sparsely distributed in the ECM hydrogel.

In the 8 mg/mL condition, the ECM appeared to still be present at 90 days with cells contained within the bioscaffold. A quantification of neural phenotypes for comparison between concentrations and time points was focused on cells within ECM hydrogel (Fig. 9). Neural progenitors infiltrated the ECM hydrogel at all concentrations by day 1, with most neural progenitors being attracted by the 8 mg/mL condition (F-10.96, $p < 0.001$). However, all groups presented with a similar percentage and density of neural progenitors in the bioscaffold at 14 and 90 days, reflecting the further infiltration of host brain cells at all time points. As neural progenitors within the hydrogel differentiated, mature neuronal markers, such as NeuN, became more prominent and steadily increased from <2% to 5% in the 3 and 4 mg/mL condition ($F = 32.92$, $p < 0.001$). The 8 mg/mL hydrogel contained only 3.6% NeuN+ cells by 90 days. Accounting for ECM volume, density of neurons showed a further distinction between 3 and 4 mg/mL ($F = 11.09$, $p < 0.001$), with the less concentrated 3 mg/mL hydrogels showing a greater neuron density with an average of 226 neurons per μL ECM hydrogel. The quantity of astrocytes (GFAP+) within the 3 and 4 mg/mL hydrogel also gradually increased with time to approximately 10% cellular content, whereas significantly fewer astrocytes were present within the 8 mg/mL preparation ($F = 14.61$, $p < 0.001$). Astrocyte density was approximately twice that of neuronal density and equivalent between both 3 and 4 mg/mL hydrogels. In contrast, oligodendrocytes were significantly increased in the 8 mg/mL condition to almost 30% of cells ($F = 13.27$, $p < 0.01$). In all ECM concentrations, oligodendrocytes increased with time and were the dominant neural phenotype by 90 days ($F = 42.12$, $p < 0.001$). However, considering the number of oligodendrocytes in relation to ECM hydrogel volume, a significantly lower density of oligodendrocytes was evident in the 8 mg/mL concentration at 90 days compared to the 3 and 4 mg/mL condition ($F = 3.78$, $p < 0.01$). Indeed, the density of oligodendrocytes was 3-fold greater than neuron density in the less concentrated gels. This phenotypic analysis of neural cells inside the ECM hydrogel shows an increasing presence of cells that are required to generate neural tissue within the bioscaffold, with predominance of oligodendrocytes. Although neurons are present, they are scarce in numbers and appear insufficient to replace functional brain tissue. Compared to 8 mg/mL hydrogel, the 3 and 4 mg/mL ECM preparations achieved a greater number of neurons and astrocytes, potentially further highlighting the favorable properties of these concentrations for inducing brain tissue restoration.

3.7. ECM biodegradation correlates with cellular density

The degree of biodegradation of the ECM hydrogel is related to the stroke cavity and the density of cells within the remaining scaffolding. At 1 day post-implantation, the remaining ECM volume was correlated to lesion volume ($r = 0.74$, $p < 0.01$, Fig. 10A). This correlation became even stronger at 90 days, with a greater spread between animals, i.e. degradation of ECM produced smaller lesion volumes, whereas a lack of degradation resulted in larger lesions ($r = 0.92$, $p < 0.01$). ECM biodegradation is therefore directly correlated with reducing the extent of a lesion cavity. To probe if ECM biodegradation is linked to cell infiltration, ECM volume was correlated with the total number of invading cells. Initially, a non-significant medium correlation ($r = 0.49$, Fig. 10B) was found. However, by 90 days, an inverse relationship ($r = -0.81$, $p < 0.001$) was evident indicating that lower amounts of ECM bioscaffolding exhibit higher cell densities. This is consistent with the observation that efficient biodegradation in the 3 and 4 mg/mL conditions was accompanied by a high cell density within the bioscaffold, whereas a low cell density was found in the 8 mg/mL hydrogel, which underwent a limited biodegradation. The gradual shift from a positive to a negative correlation is evident over time, revealing how intertwined the process of ECM biodegradation and cell density within the scaffold is.

Further correlational analyses of cell phenotypes and their relationship to ECM biodegradation also demonstrated this temporal shift. Macrophage density is initially positively correlated with ECM volume, i.e. the larger the ECM volume, the higher the density of macrophages ($r = 0.68$, $p < 0.01$. Fig. 10C). Yet, by 14 days this relationship is no longer evident ($r = -0.11$, n.s.) and by 90 days an inverse association emerged ($r = -0.68$, $p < 0.05$), with denser macrophage presence being related to less scaffolding remaining. This temporal shift was also evident for endothelial cells ($r = -0.79$, $p < 0.01$ at 90 days, Fig. 10D), neural progenitors ($r = -0.68$, $p < 0.05$ at 90 days, Fig. 10E), neurons ($r = -0.52$, $p < 0.05$ at 90 days, Fig. 10F) and oligodendrocytes ($r = -0.72$, $p < 0.01$ at 90 days, Fig. 10H). On day 1, astrocytes did not show a strong association with ECM volume ($r = 0.16$, n.s., Fig. 10G) and by 14 days post-implantation a medium size negative correlation emerged ($r = -0.57$, $p < 0.05$) indicating that better biodegradation produced more astrocytes infiltration. By 90 days, this correlation was even stronger ($r = -0.8$, $p < 0.01$). Although correlation does not imply causation, astrocytes and endothelial cells showed stronger correlations with ECM biodegradation at 90 days than macrophages, potentially highlighting their involvement in ECM hydrogel biodegradation in the brain.

Please cite this article in press as: H. Ghuman et al., Biodegradation of ECM hydrogel promotes endogenous brain tissue restoration in a rat model of stroke, Acta Biomater. (2018), https://doi.org/10.1016/j.actbio.2018.09.020

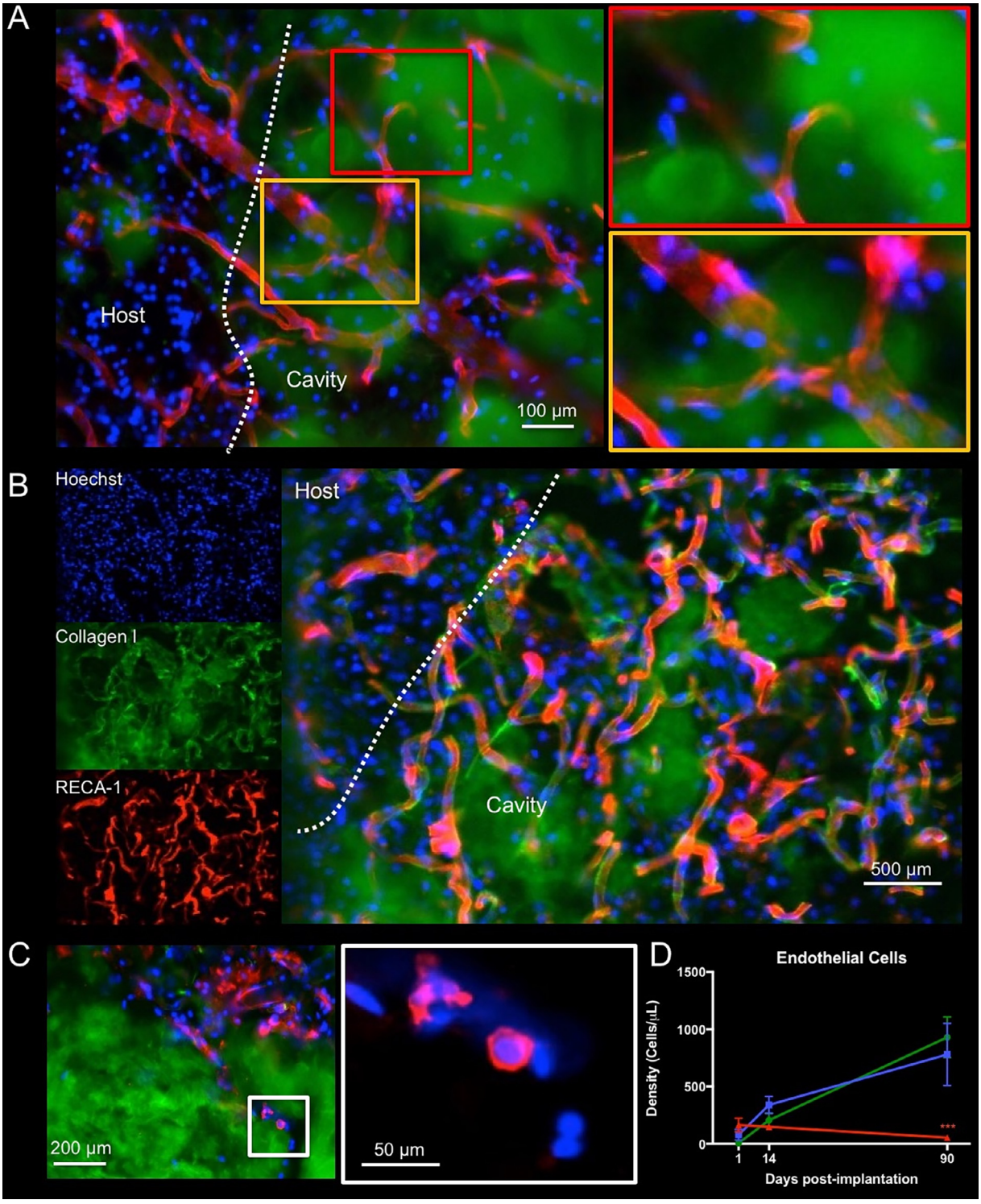

Fig. 7. Vascularization of the ECM hydrogel. A. Neovascularization inside the hydrogel was evident at 14 days if hydrogel underwent an efficient biodegradation, as illustrated here after implantation of a 3 mg/mL ECM bioscaffold. B. However, in some cases very tortuous vessels can be seen. C. Preceding the formation of vasculature is the infiltration of endothelial cells. In the 8 mg/mL condition, infiltration of endothelial cells is seen, but there is a lack of vascular formation. A higher magnification of RECA-1+ cells highlights the early stages of alignment of individual cells that invaded the hydrogel. D. A quantification of endothelial cell infiltration indicated a higher infiltration in the 8 mg/mL condition 1 day post-implantation, but a turning point is reached at 14 days where there is decrease of endothelial cells at this concentration. Endothelial cell infiltration was linearly increased in the 3 and 4 mg/mL concentrations, constituting almost 30% of all cells in the hydrogel at 90 days. ($^{***}p < 0.001$).

4. Discussion

The long-held Ramon y Cajal dogma that the brain does not have the capacity to repair [58] was refuted with the discovery of neural stem cells (NSCs) in the subependymal zone and their response to tissue damage [59]. Peri-infarct implantation of NSCs promoting behavioral recovery further demonstrated the potential to promote tissue repair using these cells [11]. The dogma that lost brain tissue cannot regenerate (i.e. form new tissue rather than replace cells) has mostly remained unchallenged [5,6]. Based on

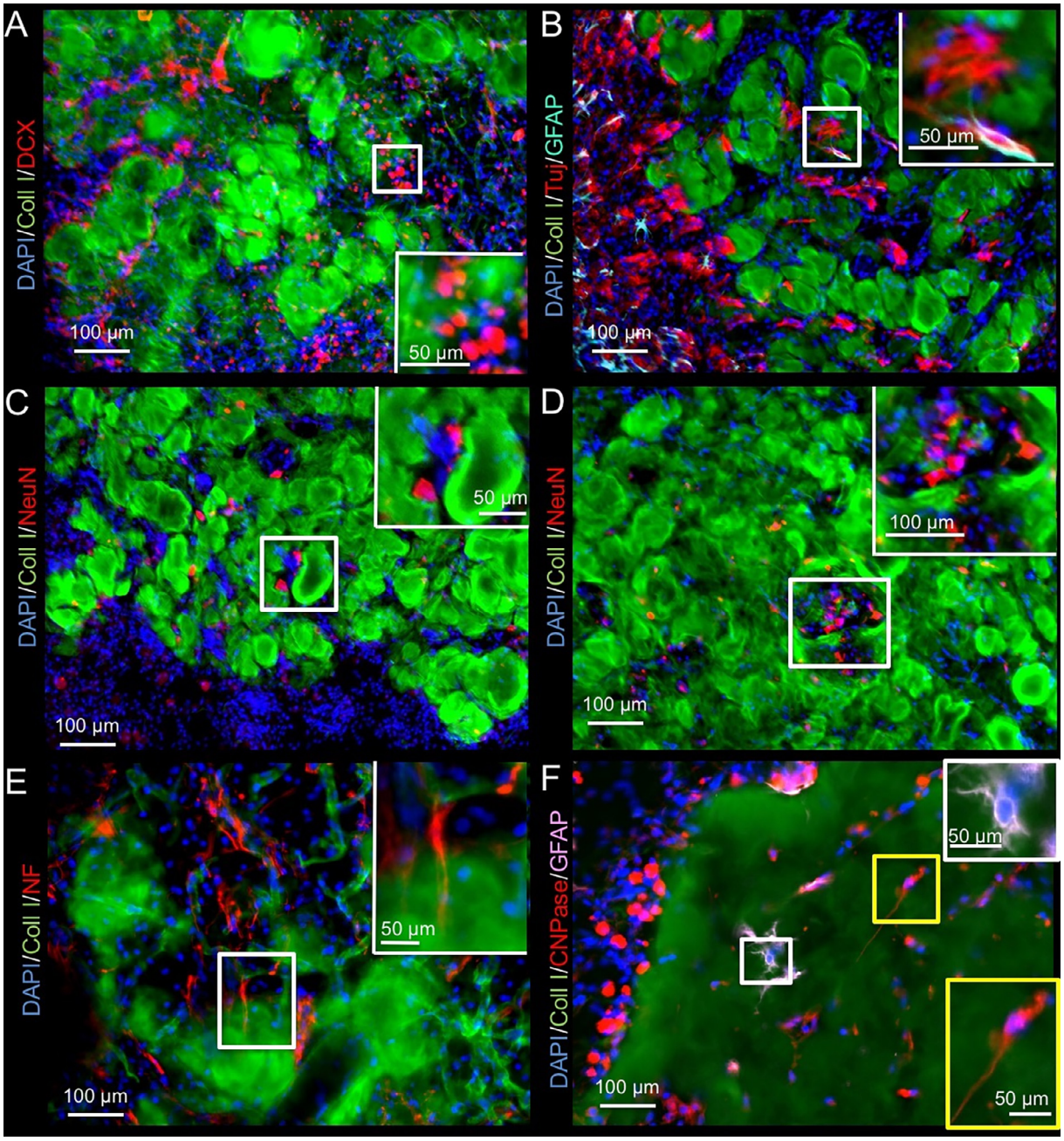

Fig. 8. Neuronal and glial cell invasion into the ECM hydrogel. A. While most of the migrating neural progenitors (doublecortin, DCX) were seen at the host-biomaterial interface, a small number of DCX+ cells could be seen inside the material (4 mg/mL shown). B. Immunostaining with beta III-tubulin (Tuj) neuron marker revealed further differentiation of these progenitors inside, as well as in between the remnant of ECM hydrogel. Occasionally GFAP+ astrocytes were adjacent to these neurons, but often these neurons were not paired with astrocytes. C. To verify if mature neurons were being generated in this de novo tissue, NeuN staining was performed to target post-mitotic neurons that typically extend processes for tissue integration. Fewer of these were evident, mostly in between ECM hydrogel patches, rather than within the scaffold per se. D. Occasional clusters containing NeuN+ cells in between ECM hydrogel were also found, potentially illustrating different stages of development within newly forming tissue. E. Neuron and tissue maturation were evident at 90 days with some neurons extending neurofilament (NF) containing axons. F. Glia lineage cells also invaded the ECM hydrogel. There were surprisingly fewer astrocytes inside the hydrogel, whereas oligodendrocytes efficiently colonized the weaker 3 and 4 mg/mL scaffolds by 90 days post-injection.

our previous work using ECM hydrogel for injection into the stroke cavity [33–35,56], the present study suggests that the brain has an endogenous potential to partially restore lost tissue if an inductive and degradable bioscaffold that can support neovascularization and infiltration of neural cells is provided. However, it remains unclear here if this de novo tissue can support behavioral recovery.

4.1. Achieving an efficient biodegradation in the brain

A concentration of >3 mg/mL of porcine UBM-ECM is required to achieve gelation and retention of the bioscaffold in a stroke lesion [33]. Increases in ECM concentration produce a stiffer and denser gel, with 8 mg/mL being equivalent to brain tissue (G′ 500–1000 Pa) [46–48]. Acute cellular infiltration in an 8 mg/mL ECM hydrogel was greater than other concentrations [34], but there was a limited 32% degradation of this concentration at 90 days [35]. This relatively slow degradation of the ECM contrasts with peripheral organs, where ECM bioscaffolds in solid configurations (such as sheets) show complete replacement within 75–90 days [36–40]. Two key questions emerge from the present study: 1) Does the brain have the same capacity to degrade ECM bioscaffolds as other organ systems, and 2) is the biodegradation

Please cite this article in press as: H. Ghuman et al., Biodegradation of ECM hydrogel promotes endogenous brain tissue restoration in a rat model of stroke, Acta Biomater. (2018), https://doi.org/10.1016/j.actbio.2018.09.020

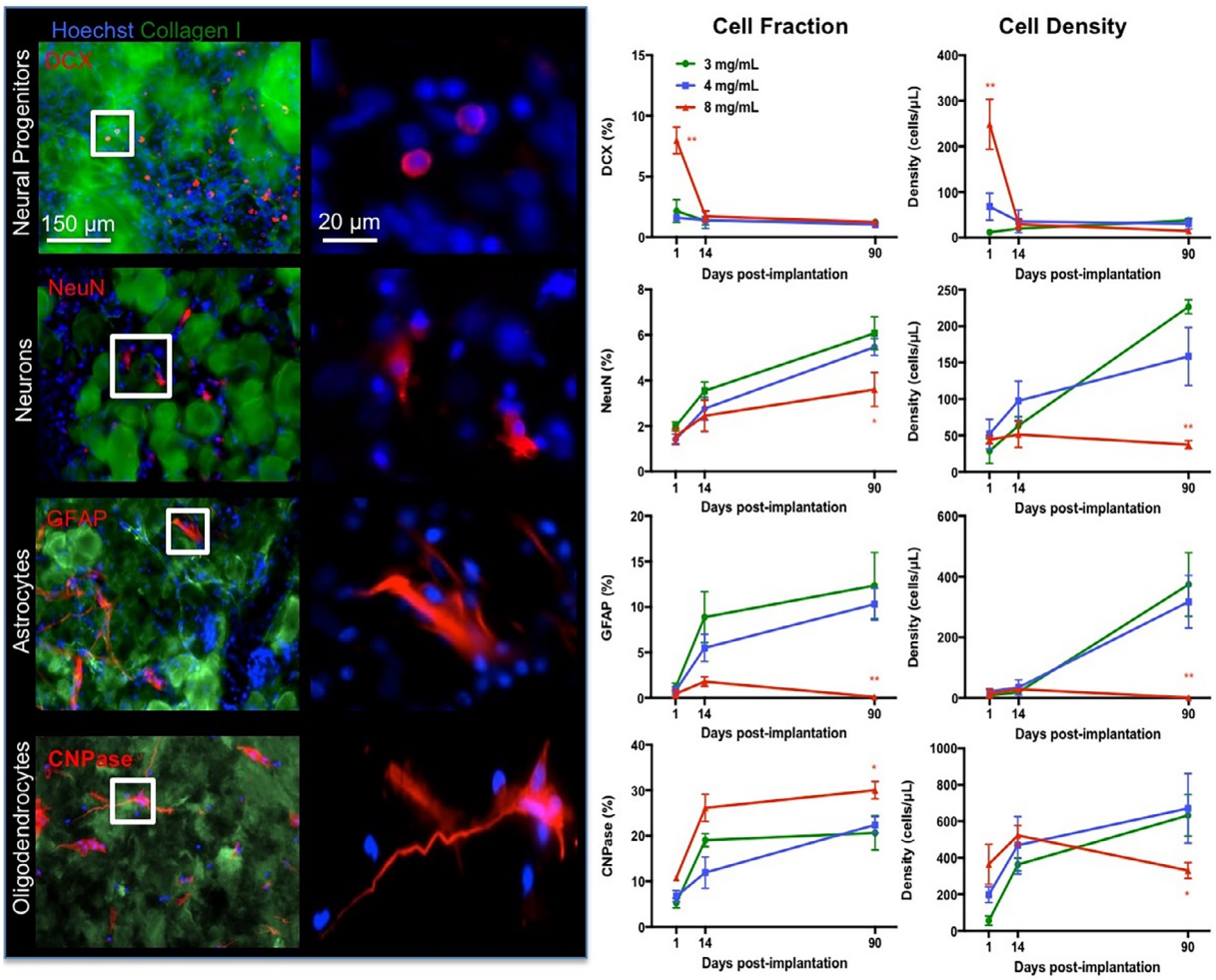

Fig. 9. Phenotypic characterization and quantification of invading neuronal cells. The proportion of neural cells 1 day post-implantation was approximately 30% with neural progenitors and oligodendrocytes being the predominant phenotypes (images show 4 mg/mL condition). The 8 mg/mL ECM hydrogel was especially efficient in attracting neural progenitors at this time point. However, the proportion of neural progenitor content reduced by 14 days, as mature phenotypes became more prominent, consistent with differentiation of cells and maturation of tissue. At 90 days, the less concentrated 3 and 4 mg/mL hydrogel contained a higher density of neurons, astrocytes and oligodendrocytes compared to the 8 mg/mL concentration. The 3 and 4 mg/mL ECM concentrations therefore provide favorable conditions for neural tissue formation. ($^{*}p < 0.05$; $^{**}p < 0.01$).

profile determined by the stiffness of the ECM hydrogel. The biodegradation characteristics in peripheral organs are mostly based on sheets of ECM, rather than hydrogel, and do not address the influence of ECM stiffness on tissue repair [60]. We investigated different concentrations of ECM hydrogels to determine the impact of their rheological properties on biodegradation at different time points. The stiffer 8 mg/mL showed a slow biodegradation, as previously reported [35], whereas the less concentrated and less stiff gels of 3 and 4 mg/mL were resorbed at a rate twice as fast, with an ~80% reduction in volume within 14 days. This biodegradation is faster than the 50% biodegradation reported at 30 days in peripheral soft tissue defects [37], but could be a reflection of differences in product formulation. Importantly, these results show that the brain is capable of ECM hydrogel degradation and that this may be influenced by stiffness of the biomaterial.

The rheological properties of the ECM hydrogel are in part determined by its density and content of inductive material. Higher concentrations of ECM hydrogel package more material into the same space producing a denser scaffold that can limit cell invasion, but also present more biomaterial to degrade for the same volume. The greater cell invasion at 1 day in the 8 mg/mL higher concentration indicates that density and stiffness of the material is not a barrier for infiltrating cells. In contrast, the results from the 3 and 4 mg/mL conditions, which contain less than half the inductive material of the 8 mg/mL condition, provide a continued cell invasion and biodegradation. Macrophage invasion was positively correlated ($r = 0.68$) with ECM volume at 24 h after implantation, but over time this relationship inverted ($r = -0.68$) with lower macrophage density being related to poor ECM degradation (i.e. larger remaining volume). We surmise therefore that stiffness and density, rather than the inductive content, of the 8 mg/mL are the main barriers to macrophage infiltration and hydrogel resorption. Ideally, these two variables (rheological properties and inductive content) can be dissociated to specifically investigate the contribution of each to cell migration and biodegradation. Although this level of experimental control can be readily achieved with synthetic polymers and peptides, the use of natural materials generally does not afford this distinction.

The inductive properties of ECM bioscaffolds remain poorly understood, although the release of chemokine factors, the release of matrix bound nanovesicles, as well as matricellular and juxtracrine signaling molecules have been all been thought to play an orchestrated role [20]. These mechanisms have led to the concept that ECM provides the "soil" to seed stem cells from the host organ [61]. However, the most effective constitution of this "soil" remains unknown, and may differ for various tissues. A comparison

Please cite this article in press as: H. Ghuman et al., Biodegradation of ECM hydrogel promotes endogenous brain tissue restoration in a rat model of stroke, Acta Biomater. (2018), https://doi.org/10.1016/j.actbio.2018.09.020

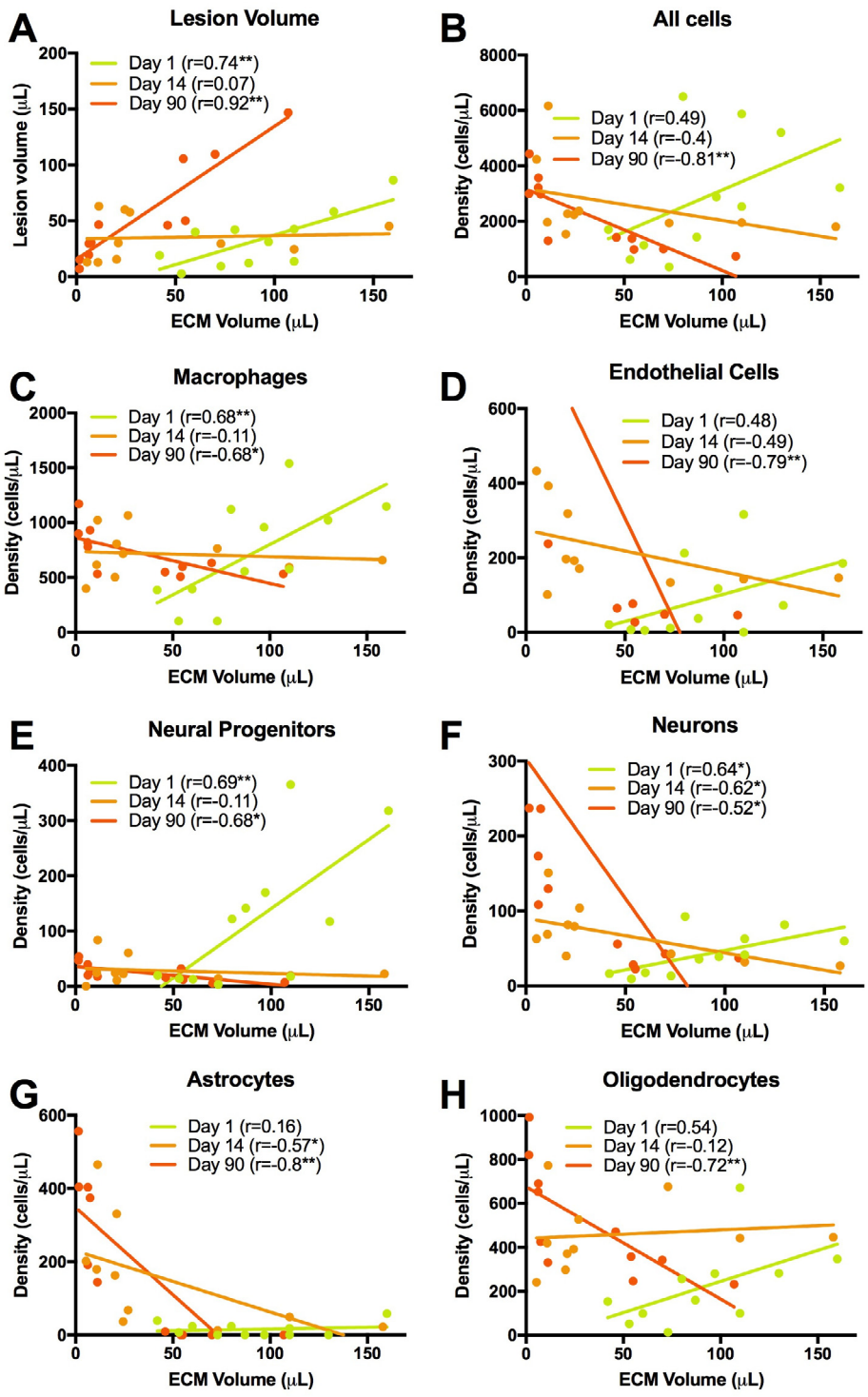

Fig. 10. Correlations of ECM hydrogel volume and cellular content. To evaluate the relationship between ECM hydrogel degradation and cellular content, a correlational analysis at each time point was performed for lesion volume (A), all invading cells (B), macrophages (C), endothelial cells (D), neural progenitors (E), neurons (F), astrocytes (G) and oligodendrocytes (H). A dramatic inversion of the relationship between ECM volume at day 1 and 90 occurred. At day 1 all measures, apart of astrocytes, revealed a positive correlation with ECM volume. On day 14, the association between ECM volume and cell content was weak, but by 90 days the relationship inverted with biodegradation of ECM (i.e. lower volume) producing greater cell content and differentiation.

of ECM hydrogels from different organs and their potential to replace lost tissue can provide a pragmatic approach to contrast favorable components [28]. A bottoms-up approach can also investigate individual components, but it might fail to replicate some of the complexities of co-stimulation that occur with natural bioscaffolds. The concept of "ground substance" has been proposed as an amorphous gel in extracellular space that contains ECM proteins that induce tissue regeneration in the absence of fibrous materials, such as collagen and elastin, which are mostly required for structural purposes [62]. Although this ground substance might vary depending on the tissue, most cell migration uses similar molecules. Molecules involved in the infiltration of cells might hence

Please cite this article in press as: H. Ghuman et al., Biodegradation of ECM hydrogel promotes endogenous brain tissue restoration in a rat model of stroke, Acta Biomater. (2018), https://doi.org/10.1016/j.actbio.2018.09.020

be well conserved between organs. In this context, it is interesting to speculate that the repair process observed here follows similar processes to those observed in wound healing [63]. A key difference is that no granulation tissue is formed in the CNS. Granulation tissue (typically rich in type III collagen) is typically weaker than actual tissue containing type I collagen [64]. This finding would concur with our observation that ECM hydrogels weaker than actual brain tissue performed better in promoting tissue regeneration. Provision of ECM hydrogel, as described here, hence would introduce a "ground substance" that serves as granulation tissue to support the infiltration of host cells and angiogenesis.

4.2. Neovascularization of a brain tissue cavity

A quintessential step in tissue engineering is the re- or neovascularization of *de novo* tissue [65]. Transplantation of NSCs attached to poly-lactic acid-co-glycolic acid (PLGA) microparticles is insufficient to efficiently vascularize newly forming tissue [18,66], but requires the secretion of vascular endothelial growth factor A (VEGF-A) to promote a neovascularization [67]. The inductive properties of ECM hydrogel are in part due to its growth factor content, including VEGF-A [21]. The higher 8 mg/mL ECM concentration attracted higher numbers of endothelial cells compared to the lower hydrogel concentrations [34], but failed to produce a robust vasculature by 90 days [35]. Incorporation of NSCs for co-delivery with ECM hydrogel also did not lead to efficient vascularization [18]. In contrast to these failures of neovascularization of the stroke cavity, here we achieved an efficient and extensive vascularization of ECM hydrogel with weaker 3 and 4 mg/mL bioscaffolds. Although these lower concentrations produced less cell invasion at 24 h post-implantation, potentially due to their lower inductive potential, the weaker gels afforded a more persistent invasion and greater organization of tubular structures within the scaffold. Neovascularization of the stroke cavity is hence possible without modification of the ECM hydrogel, with scaffold stiffness and density potentially being key determinants in promoting angiogenesis. The precise mechanisms of these processes require further investigation.

One challenge in understanding the processes leading to an efficient vascularization is the changing properties of the bioscaffold due to cell infiltration. The presence of cells, such as macrophages, leads to a greater porosity, secretion of different chemokines, but also deposition of new ECM. The invasion of endothelial cells and formation of blood vessels can also contribute to this process by providing a new route for peripheral macrophages to invade the hydrogel from within rather than through the peri-infarct tissue. At 90 days, endothelial cell density was highly correlated ($r = -0.79$) with the degree of ECM biodegradation indicating the intricate connection between these two processes. It is likely that angiogenesis and biodegradation act in conjunction with each other. It is this interaction that potentially explains the stark dichotomy between very efficiently degraded and vascularized bioscaffolds at 3 and 4 mg/mL and the 8 mg/mL concentration. Nevertheless, these differences in the time course of cellular behavior in the bioscaffold indicate the complexities of differentiating biomaterial properties and their causal influence on biological processes. Unraveling causal interactions is very challenging, but a time course analysis of cell invasion and their changing phenotypes in relation to ECM biodegradation provides novel insights into these processes and allows for the formulation of specific hypotheses that can be evaluated in more mechanistic studies.

4.3. Temporal profile of tissue regeneration after stroke damage

The migration of cells into the ECM hydrogel is a pivotal and necessary event to regenerate tissue. Acute cell infiltration indicates that a host response to hydrogel is very rapid. Not only macrophages and endothelial cells infiltrate within 24 h, but also neural lineage cells that participate in peri-infarct tissue repair. Individual chain cell migration was the predominant method of acute infiltration by "leader cells" into the bioscaffold. This individual cell migration is dependent on cell-matrix interactions involving integrins and proteases [68]. Akin to cancer cell invasion leading to a remodeling of the tissue microenvironment, chains of small files followed leader cells and more extensively remodeled the bioscaffold. Although by 24 h almost all areas of the scaffold contain individual cells, the density of cells in the scaffold shifted in the opposite directions for the 3 vs 8 mg/mL concentrations. The less concentrated gels showed a gradual increase in cell density, potentially reflecting the weaker inductive potential at the acute time point and an easier substrate to remodel for secondary chain migration. Eventually these channels of cell infiltration supported collective sheet cell migration at 14 days that led to a parcellation of the scaffold into smaller patches. This collective migration is more dependent on cell-cell interactions with the chain rather than their interaction with the bioscaffold [69]. The 4 mg/mL concentration provided conditions for a very stable cell density within the material, whereas the stiffer and denser 8 mg/mL saw a gradual decline in cell density, although it had the highest inductive potential at 24 h. If secondary cell migration in the gel is more reliant on interactions with other cells, the stiffer 8 mg/mL might be too dense to allow sufficient cell interactions to promote collective sheet cell migration. A successful cell infiltration pattern and colonialization of the bioscaffold therefore share similarities to cancer cell invasion and tissue remodeling [68], although the composition of cell phenotype is much more diverse and dynamic.

The time course of ECM biodegradation and tissue restoration in peripheral tissues indicates a predominance of macrophages in the first wave of invasion with most of these undergoing a M1-like activation and being the main source of leader cells observed in individual cell chain migration. However, a shift towards M2-like macrophages is thought to be crucial for tissue remodeling [70]. Indeed, this shift was evident in the present study between the 1 and 14 day time points. Stiffer gels were associated with a higher macrophage response [71], which is consistent with more macrophages invading the 8 mg/mL concentration at 24 h. Macrophage density within the hydrogel was key to promote a rapid biodegradation. For the 8 mg/mL concentration macrophage density decreased over time, but it consistently remained over 700 cells/μL for the 4 mg/mL and the 3 mg/mL. A plateau in macrophage number was reached by 14 days and was maintained thereafter. The 4 mg/mL condition promoted significantly less M2-like macrophages at the crucial 14 days time point. However, the peak M2-like polarization for the 4 mg/mL could have occurred between 1 and 14 days. The inductive protein content, as well as scaffold density/stiffness, are likely interacting mechanisms that govern the process of macrophage invasion and density.

In peripheral tissue, this macrophage pro-repair response is followed by host parenchymal cell infiltration. Nevertheless, we have demonstrated that by 24 h, host cells are already present within the ECM scaffold, especially DCX+ neural progenitors [34]. There is a persistent repair response in the stroke-damaged brain that is ongoing even 1 year post-infarction [10]. It is likely that these neural cells responding to repair in the damaged peri-infarct tissue are being attracted into the ECM hydrogel. Although little is known about the infiltration of neural progenitors into hydrogels, it is likely that most neural and endothelial cells will rely on the soluble SDF-1/CXCR4 signaling axis [72] and/or juxtacrine signaling by integrins (e.g. fibronectin, laminin) in the hydrogel [73]. Further mechanistic studies will be required to determine if there are key functional differences in invasion/migratory behavior between these signaling pathways in scaffold colonization. Although the ini-

Please cite this article in press as: H. Ghuman et al., Biodegradation of ECM hydrogel promotes endogenous brain tissue restoration in a rat model of stroke, Acta Biomater. (2018), https://doi.org/10.1016/j.actbio.2018.09.020

tial cell infiltration of neural progenitors was higher in the stiffer 8 mg/mL hydrogel, the less concentrated 3 and 4 mg/mL hydrogel supported better neuron and astrocyte differentiation, corroborating in vitro evidence from using cultured neural stem cells [74]. Neuronal ($r = -0.52$) and astrocytic density ($r = -0.8$) was negatively correlated with remaining ECM volume by 90 days, further indicating that efficient biodegradation observed in the less concentrated hydrogels is favorable to promote *de novo* neural tissue formation. Although glial scar formation is often seen as a barrier to tissue regeneration, it here did not prevent cell invasion or biodegradation of the bioscaffold. It has been shown by others that astrocyte scar formation aids axon regeneration in the spinal cord rather than preventing it [75]. The temporal profile of tissue regeneration after a stroke in the brain with the 3 and 4 mg/mL concentration ECM hydrogel therefore follows a similar pattern to that reported in peripheral tissues, with a predominant early macrophage response being gradually superseded by the invasion of neural cells by 14 days with over 80% of scaffolding being degraded. A rapid 2–3 week biodegradation period has been identified as one of the requirements to promote tissue regeneration [76]. However, even at 90 days post-implantation there is still ongoing evidence of structural remodeling within this newly formed tissue. These different phases are reminiscent of the processes described for natural wound healing in other tissues [77], suggesting that ECM hydrogel acts as ground substance fostering a granulation tissue in the stroke cavity.

5. Conclusions

The brain mounts a repair response to damaged tissue, but no spontaneous regeneration of lost tissue occurs [6]. Despite this, the present study suggests that implantation of ECM hydrogel can lead to an induced regeneration of brain tissue. Specifically, the 4 mg/mL hydrogel ($G' \sim 76$ Pa) has the most favorable characteristics for brain regeneration. Using this formulation, 80% of the scaffold was degraded by 14 days post-implantation at a speed of 6.11 μL/day with a persistent level of 700–800 macrophages in each μL of ECM hydrogel. The density of mature neural cells consistently increased in the remaining scaffolding, reflecting the structural remodeling phase of tissue regeneration, which was still ongoing at 90 days post-implantation. These measurements provide clear performance benchmarks to compare different scaffolds and their potential for tissue regeneration in the brain [78]. Volumetric tissue loss after a stroke can potentially be treated using this approach, but functional and behavioral studies will be needed to determine the therapeutic potential. Although further optimization and a better mechanistic understanding is required to afford greater control over the processes involved in tissue regeneration, *in situ* engineering of brain tissue using inductive biomaterials is encouraging and opens new therapeutic avenues.

6. Disclosure

The authors have no personal financial or institutional interest in any of the drugs, materials, or devices described in this article. None of the funders had a role in the design of the studies.

Acknowledgements

The study was funded in part by NINDS (R01NS08226), NIBIB (R01EB016629), Vertex Pharmaceuticals, and C.R. Bard. ARM was supported by a fellowship from CAPES Foundation, Brazil.

References

[1] J.A. Baddour, K. Sousounis, P.A. Tsonis, Organ repair and regeneration: an overview, Birth Defects Res. C Embryo Today 96 (1) (2012) 1–29.
[2] G.K. Michalopoulos, M.C. DeFrances, Liver regeneration, Science 276 (5309) (1997) 60–66.
[3] I. Bechmann, Failed central nervous system regeneration: a downside of immune privilege?, Neuromol Med. 7 (3) (2005) 217–228.
[4] E.M. Tanaka, P. Ferretti, Considering the evolution of regeneration in the central nervous system, Nat. Rev. Neurosci. 10 (10) (2009) 713–723.
[5] E.J. Fry, Central nervous system regeneration: mission impossible?, Clin Exp. Pharmacol. Physiol. 28 (4) (2001) 253–258.
[6] L.S. Illis, Central nervous system regeneration does not occur, Spinal Cord 50 (4) (2012) 259–263.
[7] F. Moreau, S. Patel, M.L. Lauzon, C.R. McCreary, M. Goyal, R. Frayne, A.M. Demchuk, S.B. Coutts, E.E. Smith, Cavitation after acute symptomatic lacunar stroke depends on time, location, and MRI sequence, Stroke 43 (7) (2012) 1837–1842.
[8] M.V. Sofroniew, H.V. Vinters, Astrocytes: biology and pathology, Acta Neuropathol. 119 (1) (2010) 7–35.
[9] D. Katsman, J. Zheng, K. Spinelli, S.T. Carmichael, Tissue microenvironments within functional cortical subdivisions adjacent to focal stroke, J. Cereb. Blood Flow Metab. 23 (9) (2003) 997–1009.
[10] I. Kazanis, N. Gorenkova, J.W. Zhao, R.J. Franklin, M. Modo, C. Ffrench-Constant, The late response of rat subependymal zone stem and progenitor cells to stroke is restricted to directly affected areas of their niche, Exp. Neurol. 248 (2013) 387–397.
[11] E.J. Smith, R.P. Stroemer, N. Gorenkova, M. Nakajima, W.R. Crum, E. Tang, L. Stevanato, J.D. Sinden, M. Modo, Implantation site and lesion topology determine efficacy of a human neural stem cell line in a rat model of chronic stroke, Stem Cells 30 (4) (2012) 785–796.
[12] M. Grabowski, B.B. Johansson, P. Brundin, Survival of fetal neocortical grafts implanted in brain infarcts of adult rats: the influence of postlesion time and age of donor tissue, Exp. Neurol. 127 (1) (1994) 126–136.
[13] M. Grabowski, R.H. Christofferson, P. Brundin, B.B. Johansson, Vascularization of fetal neocortical grafts implanted in brain infarcts in spontaneously hypertensive rats, Neuroscience 51 (3) (1992) 673–682.
[14] J.C. Sorensen, M. Grabowski, J. Zimmer, B.B. Johansson, Fetal neocortical tissue blocks implanted in brain infarcts of adult rats interconnect with the host brain, Exp. Neurol. 138 (2) (1996) 227–235.
[15] M. Grabowski, P. Brundin, B.B. Johansson, Functional integration of cortical grafts placed in brain infarcts of rats, Ann. Neurol. 34 (3) (1993) 362–368.
[16] M. Grabowski, P. Brundin, B.B. Johansson, Fetal neocortical grafts implanted in adult hypertensive rats with cortical infarcts following a middle cerebral artery occlusion: ingrowth of afferent fibers from the host brain, Exp. Neurol. 116 (2) (1992) 105–121.
[17] M. Grabowski, J.C. Sorensen, B. Mattsson, J. Zimmer, B.B. Johansson, Influence of an enriched environment and cortical grafting on functional outcome in brain infarcts of adult rats, Exp. Neurol. 133 (1) (1995) 96–102.
[18] E. Bible, F. Dell'Acqua, B. Solanky, A. Balducci, P.M. Crapo, S.F. Badylak, E.T. Ahrens, M. Modo, Non-invasive imaging of transplanted human neural stem cells and ECM scaffold remodeling in the stroke-damaged rat brain by (19)F- and diffusion-MRI, Biomaterials 33 (10) (2012) 2858–2871.
[19] B.N. Brown, S.F. Badylak, Extracellular matrix as an inductive scaffold for functional tissue reconstruction, Transl. Res. 163 (4) (2014) 268–285.
[20] I.T. Swinehart, S.F. Badylak, Extracellular matrix bioscaffolds in tissue remodeling and morphogenesis, Dev. Dyn. 245 (3) (2016) 351–360.
[21] P.M. Crapo, C.J. Medberry, J.E. Reing, S. Tottey, Y. van der Merwe, K.E. Jones, S.F. Badylak, Biologic scaffolds composed of central nervous system extracellular matrix, Biomaterials 33 (13) (2012) 3539–3547.
[22] P.M. Crapo, S. Tottey, P.F. Slivka, S.F. Badylak, Effects of biologic scaffolds on human stem cells and implications for CNS tissue engineering, Tissue Eng. Part A 20 (1–2) (2014) 313–323.
[23] J.L. Dziki, D.S. Wang, C. Pineda, B.M. Sicari, T. Rausch, S.F. Badylak, Solubilized extracellular matrix bioscaffolds derived from diverse source tissues differentially influence macrophage phenotype, J. Biomed. Mater. Res. A 105 (1) (2017) 138–147.
[24] A. Faust, A. Kandakatla, Y. van der Merwe, T. Ren, L. Huleihel, G. Hussey, J.D. Naranjo, S. Johnson, S. Badylak, M. Steketee, Urinary bladder extracellular matrix hydrogels and matrix-bound vesicles differentially regulate central nervous system neuron viability and axon growth and branching, J. Biomater. Appl. 31 (9) (2017) 1277–1295.
[25] D.O. Freytes, J. Martin, S.S. Velankar, A.S. Lee, S.F. Badylak, Preparation and rheological characterization of a gel form of the porcine urinary bladder matrix, Biomaterials 29 (11) (2008) 1630–1637.
[26] Z. Koci, K. Vyborny, J. Dubisova, I. Vackova, A. Jager, O. Lunov, K. Jirakova, S. Kubinova, Extracellular matrix hydrogel derived from human umbilical cord as a scaffold for neural tissue repair and its comparison with extracellular matrix from porcine tissues, Tissue Eng. Part C Methods 23 (6) (2017) 333–345.
[27] T.A. Prest, E. Yeager, S.T. LoPresti, E. Zygelyte, M.J. Martin, L. Dong, A. Gibson, O. O. Olutoye, B.N. Brown, J. Cheetham, Nerve-specific, xenogeneic extracellular matrix hydrogel promotes recovery following peripheral nerve injury, J. Biomed. Mater. Res. A 106 (2) (2018) 450–459.
[28] D. Tukmachev, S. Forostyak, Z. Koci, K. Zaviskova, I. Vackova, K. Vyborny, I. Sandvig, A. Sandvig, C.J. Medberry, S.F. Badylak, E. Sykova, S. Kubinova,

Injectable Extracellular Matrix Hydrogels as Scaffolds for Spinal Cord Injury Repair, Tissue Eng. Part A 22 (3–4) (2016) 306–317.
[29] C.J. Medberry, P.M. Crapo, B.F. Siu, C.A. Carruthers, M.T. Wolf, S.P. Nagarkar, V. Agrawal, K.E. Jones, J. Kelly, S.A. Johnson, S.S. Velankar, S.C. Watkins, M. Modo, S.F. Badylak, Hydrogels derived from central nervous system extracellular matrix, Biomaterials 34 (4) (2013) 1033–1040.
[30] L. Huleihel, J.L. Dziki, J.G. Bartolacci, T. Rausch, M.E. Scarritt, M.C. Cramer, T. Vorobyov, S.T. LoPresti, I.T. Swineheart, L.J. White, B.N. Brown, S.F. Badylak, Macrophage phenotype in response to ECM bioscaffolds, Semin. Immunol. 29 (2017) 2–13.
[31] Y. Wu, J. Wang, Y. Shi, H. Pu, R.K. Leak, A.K. Liou, S.F. Badylak, Z. Liu, J. Zhang, J. Chen, L. Chen, Implantation of Brain-derived extracellular matrix enhances neurological recovery after traumatic brain injury, Cell Transplant. (2016).
[32] L. Zhang, F. Zhang, Z. Weng, B.N. Brown, H. Yan, X.M. Ma, P.S. Vosler, S.F. Badylak, C.E. Dixon, X.T. Cui, J. Chen, Effect of an inductive hydrogel composed of urinary bladder matrix upon functional recovery following traumatic brain injury, Tissue Eng. Part A 19 (17–18) (2013) 1909–1918.
[33] A.R. Massensini, H. Ghuman, L.T. Saldin, C.J. Medberry, T.J. Keane, F.J. Nicholls, S.S. Velankar, S.F. Badylak, M. Modo, Concentration-dependent rheological properties of ECM hydrogel for intracerebral delivery to a stroke cavity, Acta Biomater. 27 (2015) 116–130.
[34] H. Ghuman, A.R. Massensini, J. Donnelly, S.M. Kim, C.J. Medberry, S.F. Badylak, M. Modo, ECM hydrogel for the treatment of stroke: characterization of the host cell infiltrate, Biomaterials 91 (2016) 166–181.
[35] H. Ghuman, M. Gerwig, F.J. Nicholls, J.R. Liu, J. Donnelly, S.F. Badylak, M. Modo, Long-term retention of ECM hydrogel after implantation into a sub-acute stroke cavity reduces lesion volume, Acta Biomater. 63 (2017) 50–63.
[36] J.E. Valentin, A.M. Stewart-Akers, T.W. Gilbert, S.F. Badylak, Macrophage participation in the degradation and remodeling of extracellular matrix scaffolds, Tissue Eng. Part A 15 (7) (2009) 1687–1694.
[37] R.D. Record, D. Hillegonds, C. Simmons, R. Tullius, F.A. Rickey, D. Elmore, S.F. Badylak, In vivo degradation of 14C-labeled small intestinal submucosa (SIS) when used for urinary bladder repair, Biomaterials 22 (19) (2001) 2653–2659.
[38] T.W. Gilbert, A.M. Stewart-Akers, S.F. Badylak, A quantitative method for evaluating the degradation of biologic scaffold materials, Biomaterials 28 (2) (2007) 147–150.
[39] C.L. Dearth, P.F. Slivka, S.A. Stewart, T.J. Keane, J.K. Tay, R. Londono, Q. Goh, F.X. Pizza, S.F. Badylak, Inhibition of COX1/2 alters the host response and reduces ECM scaffold mediated constructive tissue remodeling in a rodent model of skeletal muscle injury, Acta Biomater. 31 (2016) 50–60.
[40] L.E. Carey, C.L. Dearth, S.A. Johnson, R. Londono, C.J. Medberry, K.A. Daly, S.F. Badylak, In vivo degradation of 14C-labeled porcine dermis biologic scaffold, Biomaterials 35 (29) (2014) 8297–8304.
[41] B.N. Brown, S.F. Badylak, Expanded applications, shifting paradigms and an improved understanding of host-biomaterial interactions, Acta Biomater. 9 (2) (2013) 4948–4955.
[42] L.T. Saldin, M.C. Cramer, S.S. Velankar, L.J. White, S.F. Badylak, Extracellular matrix hydrogels from decellularized tissues: structure and function, Acta Biomater. 49 (2017) 1–15.
[43] P.M. Crapo, T.W. Gilbert, S.F. Badylak, An overview of tissue and whole organ decellularization processes, Biomaterials 32 (12) (2011) 3233–3243.
[44] H. Marcal, T. Ahmed, S.F. Badylak, S. Tottey, L.J. Foster, A comprehensive protein expression profile of extracellular matrix biomaterial derived from porcine urinary bladder, Regen. Med. 7 (2) (2012) 159–166.
[45] L. Huleihel, G.S. Hussey, J.D. Naranjo, L. Zhang, J.L. Dziki, N.J. Turner, D.B. Stolz, S.F. Badylak, Matrix-bound nanovesicles within ECM bioscaffolds, Sci. Adv. 2 (6) (2016) e1600502.
[46] E.R. Aurand, J. Wagner, C. Lanning, K.B. Bjugstad, Building biocompatible hydrogels for tissue engineering of the brain and spinal cord, J. Funct. Biomater. 3 (4) (2012) 839–863.
[47] A. Gefen, S.S. Margulies, Are in vivo and in situ brain tissues mechanically similar?, J Biomech. 37 (9) (2004) 1339–1352.
[48] Z. Taylor, K. Miller, Reassessment of brain elasticity for analysis of biomechanisms of hydrocephalus, J. Biomech. 37 (8) (2004) 1263–1269.
[49] M. Modo, Long-term survival and serial assessment of stroke damage and recovery – practical and methodological considerations, J. Exp. Stroke Transl. Med. 2 (2) (2009) 52–68.
[50] M. Modo, R.P. Stroemer, E. Tang, T. Veizovic, P. Sowniski, H. Hodges, Neurological sequelae and long-term behavioural assessment of rats with transient middle cerebral artery occlusion, J. Neurosci. Methods 104 (1) (2000) 99–109.
[51] E. Bible, D.Y. Chau, M.R. Alexander, J. Price, K.M. Shakesheff, M. Modo, Attachment of stem cells to scaffold particles for intra-cerebral transplantation, Nat. Protoc. 4 (10) (2009) 1440–1453.
[52] M. Ashioti, J.S. Beech, A.S. Lowe, M.B. Hesselink, M. Modo, S.C. Williams, Multi-modal characterisation of the neocortical clip model of focal cerebral ischaemia by MRI, behaviour and immunohistochemistry, Brain Res. 1145 (2007) 177–189.
[53] M. Stille, E.J. Smith, W.R. Crum, M. Modo, 3D reconstruction of 2D fluorescence histology images and registration with in vivo MR images: application in a rodent stroke model, J. Neurosci. Methods 219 (1) (2013) 27–40.
[54] W. Goldsmith, The state of head injury biomechanics: past, present, and future: part 1, Crit. Rev. Biomed. Eng. 29 (5–6) (2001) 441–600.
[55] H.W. Soon, A. Qiu, Individualized diffeomorphic mapping of brains with large cortical infarcts, Magn. Reson. Imaging 33 (1) (2015) 110–123.
[56] T. Jin, F.J. Nicholls, W.R. Crum, H. Ghuman, S.F. Badylak, M. Modo, Diamagnetic chemical exchange saturation transfer (diaCEST) affords magnetic resonance imaging of extracellular matrix hydrogel implantation in a rat model of stroke, Biomaterials 113 (2017) 176–190.
[57] D. Ito, K. Tanaka, S. Suzuki, T. Dembo, Y. Fukuuchi, Enhanced expression of Iba1, ionized calcium-binding adapter molecule 1, after transient focal cerebral ischemia in rat brain, Stroke 32 (5) (2001) 1208–1215.
[58] S. Ramony Cajal, Degeneration and Regeneration of the Nervous System, Haffner Publishing, New York City, NY, 1928.
[59] A.F. Hallbergson, C. Gnatenco, D.A. Peterson, Neurogenesis and brain injury: managing a renewable resource for repair, J. Clin. Invest. 112 (8) (2003) 1128–1133.
[60] S.F. Badylak, D.O. Freytes, T.W. Gilbert, Extracellular matrix as a biological scaffold material: structure and function, Acta Biomater. 5 (1) (2009) 1–13.
[61] S.J. Forbes, N. Rosenthal, Preparing the ground for tissue regeneration: from mechanism to therapy, Nat. Med. 20 (8) (2014) 857–869.
[62] D.N. Wheatley, Diffusion, perfusion and the exclusion principles in the structural and functional organization of the living cell: reappraisal of the properties of the 'ground substance', J. Exp. Biol. 206 (Pt 12) (2003) 1955–1961.
[63] K.S. Midwood, L.V. Williams, J.E. Schwarzbauer, Tissue repair and the dynamics of the extracellular matrix, Int. J. Biochem. Cell Biol. 36 (6) (2004) 1031–1037.
[64] L. Hakkinen, H. Larjava, L. Koivisto, Granulation tissue formation and remodeling, Endod. Top. 24 (1) (2011) 94–129.
[65] M.M. Martino, S. Brkic, E. Bovo, M. Burger, D.J. Schaefer, T. Wolff, L. Gurke, P.S. Briquez, H.M. Larsson, R. Gianni-Barrera, J.A. Hubbell, A. Banfi, Extracellular matrix and growth factor engineering for controlled angiogenesis in regenerative medicine, Front. Bioeng. Biotechnol. 3 (2015) 45.
[66] E. Bible, D.Y. Chau, M.R. Alexander, J. Price, K.M. Shakesheff, M. Modo, The support of neural stem cells transplanted into stroke-induced brain cavities by PLGA particles, Biomaterials 30 (16) (2009) 2985–2994.
[67] E. Bible, O. Qutachi, D.Y. Chau, M.R. Alexander, K.M. Shakesheff, M. Modo, Neo-vascularization of the stroke cavity by implantation of human neural stem cells on VEGF-releasing PLGA microparticles, Biomaterials 33 (30) (2012) 7435–7446.
[68] P. Friedl, S. Alexander, Cancer invasion and the microenvironment: plasticity and reciprocity, Cell 147 (5) (2011) 992–1009.
[69] P. Friedl, J.A. Zallen, Dynamics of cell-cell and cell-matrix interactions in morphogenesis, regeneration and cancer, Curr. Opin. Cell Biol. 22 (5) (2010) 557–559.
[70] B.N. Brown, R. Londono, S. Tottey, L. Zhang, K.A. Kukla, M.T. Wolf, K.A. Daly, J.E. Reing, S.F. Badylak, Macrophage phenotype as a predictor of constructive remodeling following the implantation of biologically derived surgical mesh materials, Acta Biomater. 8 (3) (2012) 978–987.
[71] A.K. Blakney, M.D. Swartzlander, S.J. Bryant, The effects of substrate stiffness on the in vitro activation of macrophages and in vivo host response to poly (ethylene glycol)-based hydrogels, J. Biomed. Mater. Res. A 100 (6) (2012) 1375–1386.
[72] S. Prokoph, E. Chavakis, K.R. Levental, A. Zieris, U. Freudenberg, S. Dimmeler, C. Werner, Sustained delivery of SDF-1alpha from heparin-based hydrogels to attract circulating pro-angiogenic cells, Biomaterials 33 (19) (2012) 4792–4800.
[73] J. Lam, N.F. Truong, T. Segura, Design of cell-matrix interactions in hyaluronic acid hydrogel scaffolds, Acta Biomater. 10 (4) (2014) 1571–1580.
[74] A. Banerjee, M. Arha, S. Choudhary, R.S. Ashton, S.R. Bhatia, D.V. Schaffer, R.S. Kane, The influence of hydrogel modulus on the proliferation and differentiation of encapsulated neural stem cells, Biomaterials 30 (27) (2009) 4695–4699.
[75] M.A. Anderson, J.E. Burda, Y. Ren, Y. Ao, T.M. O'Shea, R. Kawaguchi, G. Coppola, B.S. Khakh, T.J. Deming, M.V. Sofroniew, Astrocyte scar formation aids central nervous system axon regeneration, Nature 532 (7598) (2016) 195–200.
[76] I.V. Yannas, Emerging rules for inducing organ regeneration, Biomaterials 34 (2) (2013) 321–330.
[77] R. Shechter, M. Schwartz, CNS sterile injury: just another wound healing?, Trends Mol Med. 19 (3) (2013) 135–143.
[78] J.M. Aamodt, D.W. Grainger, Extracellular matrix-based biomaterial scaffolds and the host response, Biomaterials 86 (2016) 68–82.

Please cite this article in press as: H. Ghuman et al., Biodegradation of ECM hydrogel promotes endogenous brain tissue restoration in a rat model of stroke, Acta Biomater. (2018), https://doi.org/10.1016/j.actbio.2018.09.020